Summer 8-7-2012

Time Resolved Absorption Spectroscopy for the Study of Electron Transfer Processes in Photosynthetic Systems

Hiroki Makita
Georgia State University

TIME RESOLVED ABSORPTION SPECTROSCOPY FOR THE STUDY OF ELECTRON TRANSFER PROCESSES IN PHOTOSYNTHETIC SYSTEMS

by

HIROKI MAKITA

Under the Direction of Professor Gary Hastings

ABSTRACT

Transient absorption spectroscopy was used to study light induced electron transfer processes in Type 1 photosynthetic reaction centers. Flash induced absorption changes were probed at 800, 703 and 487 nm, and on multiple timescales from nanoseconds to tens of milliseconds. Both wild type and *menB* mutant photosystem I reaction centers from the cyanobacterium *Synechocystis* sp. PCC 6803 were studied. Photosystem I reaction centers from the green algae *Chlamydomonas reinhardtii*, and the newly discovered chlorophyll-d containing organism *Acaryochloris marina*, were also studied.

The flash induced absorption changes obtained for *menB* mutant photosystem I reaction centers are distinguishable from wild type at 800 nm. *MenB* mutant photosystem I reaction centers displays a large amplitude decay phase with lifetime of ~50 ns which is absent in wild type photosystem I reaction centers. It is hypothesized that this ~50 ns phase is due to the formation of the triplet state of primary electron donor.

INDEX WORDS: Photosynthesis, Photosystem I, P700, Laser flash photolysis, Pump-probe spectroscopy, *Synechocystis* sp. PCC 6803, *menB*, *Chlamydomonas reinhardtii*, P740, *Acaryochloris marina*

TIME RESOLVED ABSORPTION SPECTROSCOPY FOR THE STUDY OF ELECTRON TRANSFER PROCESSES IN PHOTOSYNTHETIC SYSTEMS

by

HIROKI MAKITA

A Thesis Submitted in Partial Fulfillment of the Requirements for the Degree of

Master of Science

in the College of Arts and Sciences

Georgia State University

2012

TIME RESOLVED ABSORPTION SPECTROSCOPY FOR THE STUDY OF ELECTRON TRANSFER PROCESSES IN PHOTOSYNTHETIC SYSTEMS

by

HIROKI MAKITA

Committee Chair: Gary Hastings

Committee: Vadym Apalkov

Gennady Cymbalyuk

Mukesh Dhamala

Electronic Version Approved:

Office of Graduate Studies

College of Arts and Sciences

Georgia State University

August 2012

ACKNOWLEDGEMENTS

First of all, I would like to express my gratitude to my advisor, Dr. Gary Hastings, for his patience and understanding. Without his support and guidance, this thesis would not have been possible.

I would like to thank my thesis committee members, Dr. Vadym Apalkov, Dr. Gennady Cymbalyuk, and Dr. Mukesh Dhamala for their time and support. My gratitude also goes to my lab mates, Nan Zhao and Dr. Hari Lamichhane, for their helpful suggestions.

Finally, I would like to thank the late Dr. William H. Nelson, who was my first scientific advisor at Georgia State University.

TABLE OF CONTENTS

LIST OF TABLES

LIST OF FIGURES

1 INTRODUCTION

1.1 Photosynthesis

Photosynthesis is an important biological process that occurs in plants, algae, and certain strains of bacteria. Photosynthesis is directly or indirectly responsible for nearly all food and fuel products available on earth. Photosynthesis is also directly responsible for the earth's oxygen rich atmosphere. The importance of this biological process cannot be overstated.

Photosynthesis is the term that is used to describe the set of processes that utilize solar energy to synthesis carbohydrate (biomass) from simpler molecules. In oxygenic photosynthesis carbohydrate is synthesized from carbon dioxide and water. The overall oxygenic photosynthetic process can be summarized as:

$$6\,CO_2 + 6\,H_2O \xrightarrow[plant]{light} C_6H_{12}O_6 + 6\,O_2$$

The photosynthetic process is also outlined schematically in figure 1.1.

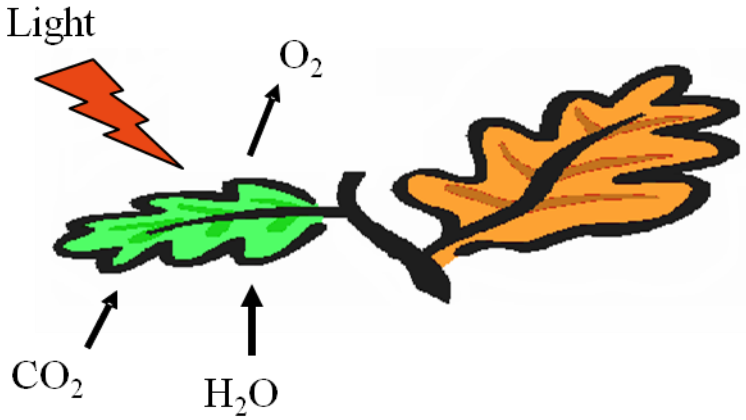

Figure 1.1 Simple schematic showing the overall photosynthetic process in a plant

Photosynthetic processes are generally divided into two parts. One part requires light while the other does not. In the "light reactions" water is split into molecular oxygen. The protons and electrons from this water splitting are used to make ATP and NADPH (from ADP and NADP) [1]. These latter products of the light reactions are utilized in a series of "dark reactions" that ultimately lead to the reduction of carbon dioxide to glucose [1]. In this thesis the focus is on only certain aspects of the light reactions.

1.2 The Light Reactions

In plants, photosynthetic processes occur inside large cellular organelles called chloroplasts [1]. The light and dark reactions occur in spatially distinct regions inside the chloroplasts. The light reactions occur in a series of stacked membranes called the thylakoid membrane. In the regions of the thylakoid membrane where the light reactions occur there are four protein complexes that function cooperatively to split water and reduce NADP (and produce ATP). The four protein complexes are called: photosystem II (PSII), cytochrome b6-f, photosystem I (PSI), and ATP synthase (Figure1.2).

Photosystems II and I are large membrane spanning protein complexes that contain or bind a large number of chlorophyll molecules/pigments that absorb solar energy. The light reactions begin when light energy or solar photons are absorbed by PSII. The light energy is used to transfer electrons vectorially across the thylakoid membrane via a series of bound pigment acceptors (Figure 1.2). The electrons are transferred from PSII to the cytochrome b6-f complex, and to PSI. The electrons receive the light energy again at PSI as the complex absorbs the light. The electrons travel through PSI and across the membrane and is ultimately accepted by NADP in stroma, which is reduced to NADPH. Transferring electrons across the thylakoid membrane generates an electrical potential difference across the membrane. This potential

gradient across the membrane is used by ATP synthase to make ATP. The end products, ATP and NADPH, are then spent in the dark reactions to reduce CO_2 to carbohydrate. Of four major protein complexes involved in the light reactions, photosystem I is focused on in this thesis.

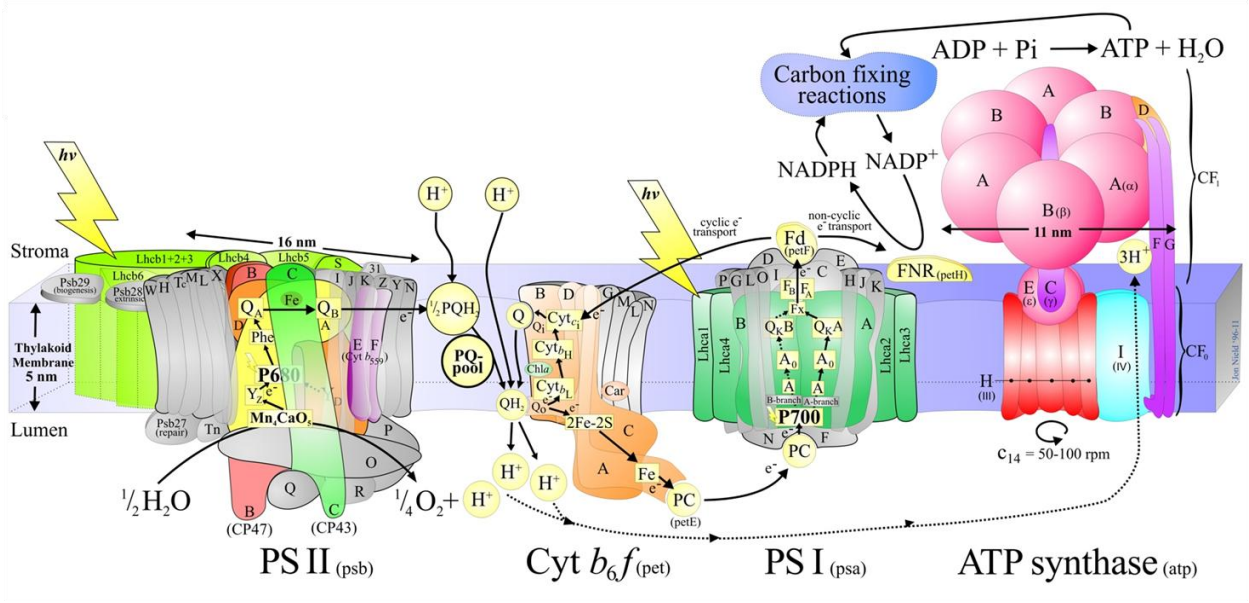

Figure 1.2 A detailed schematic model of the higher plant / green algal thylakoid membrane with major protein complexes involved in oxygenic photosynthesis. Taken from http://www.photosynthesis.sbcs.qmul.ac.uk/nield/psIIimages/oxygenicphotosynthmodel.html [1]

1.3 Structure of Photosystem I

Photosystem I is a membrane spanning protein complex that catalyzes light induced electron transfer across the thylakoid membrane. The cyanobacterial PSI is composed of 12 protein subunits, 96 chlorophylls, 22 carotenoids, 3 iron-sulfur clusters, 2 phylloquinones, and 4 lipids [2].

In higher plants and algae, the collection of incident light is achieved by functional units called light-harvesting complexes (Lhc in Figure 1.2), which are found in the exterior region of PSI. The light-harvesting complexes contain large numbers of chlorophyll and carotenoid molecules. These pigment molecules are called antenna pigments. The antenna pigments absorb

light energy, and transfer it to the inner protein complex of PSI through the process of resonance energy transfer. Between pigments in cyanobacteria instead of light harvesting complexes, 90 chlorophyll molecules and 22 carotenoids capture and transfer light energy. The inner complex where the energy is transferred is called a reaction center (RC).

The reaction center, the core complex of PSI and the location of the primary photochemistry transfers the electrons it receives from cytochrome through a series of its acceptors to ferredoxin located on the stromal side of the thylakoid membrane. Of the twelve protein subunits in the PSI core complex, nine of them: *PsaA, PsaB, PsaF, PSaI, PsaJ, PSaK, PSaL, PsaM,* and *PsaX,* form trans-membrane subunits. The three remaining subunits, *PsaC, PsaD,* and *PsaF* are bound on the stromal side (Figure 1.3).

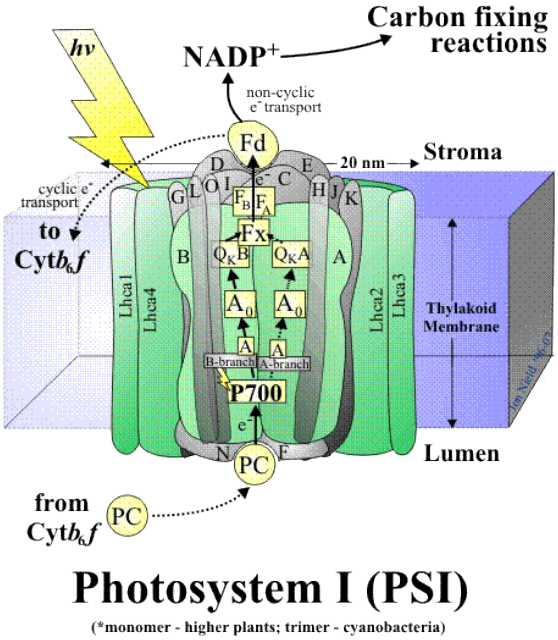

Figure 1.3 A schematic depicting the architecture of the PSI core complex embedded in the thylakoid membrane. The possible routes of electron transfer are shown with arrows. The subunits are labeled with alphabets. Taken from http://www.photosynthesis.sbcs.qmul.ac.uk/nield/psIIimages/PSI.html [3]

The protein co-factors involved in the electron transfer are 6 chlorophyll molecules, 2 phylloquinones, and 3 iron-sulfur clusters. The co-factors are arranged along two symmetric branches, called A and B branches. Most co-factors of electron transfer, including antenna pigments (90 chlorophylls and 22 carotenoids), are bound to heterodimer subunits of *PsaA* and *PsaB.* At the base of *PsaA* and *PsaB* on the lumenal side, positions labeled eC-A1 and eC-B1, is P700. P700, heterodimer formed by chlorophyll *a* and chlorophyll-*a'*, is the primary electron donor named after its maximum absorbance at 700 nm. Chlrophyll-*a'* is a 13^2 epimer of chlorophyll-*a* (Figure1.4.b, Figure 1.5). The two chlorophylls are oriented parallel to each other and perpendicular to the membrane plane. P700 receives light energy from the surrounding antenna pigments, and rapidly transfers electrons to the primary electron acceptor A_0. Before the primary electron acceptor is a pair of chlorophyll molecules designated at eC-B2 and eC-A2. This pair of chlorophyll are not involved in the electron transfer. The primary electron acceptors are chlorophyll-*a* molecules at eC-A3 and eC-B3. The secondary electron acceptors A_1 are phylloquinone (Vitamin K_1) molecules (Figure1.4.a). The primary and secondary electron acceptors are found on both side of the A and B branches. The secondary electron acceptors transfer electrons to the three iron-sulfur clusters, F_x, F_A, and F_B. F_x, the iron-sulfur positioned closest to the secondary electron acceptors, is aligned along the axis of the symmetry of the two branches.

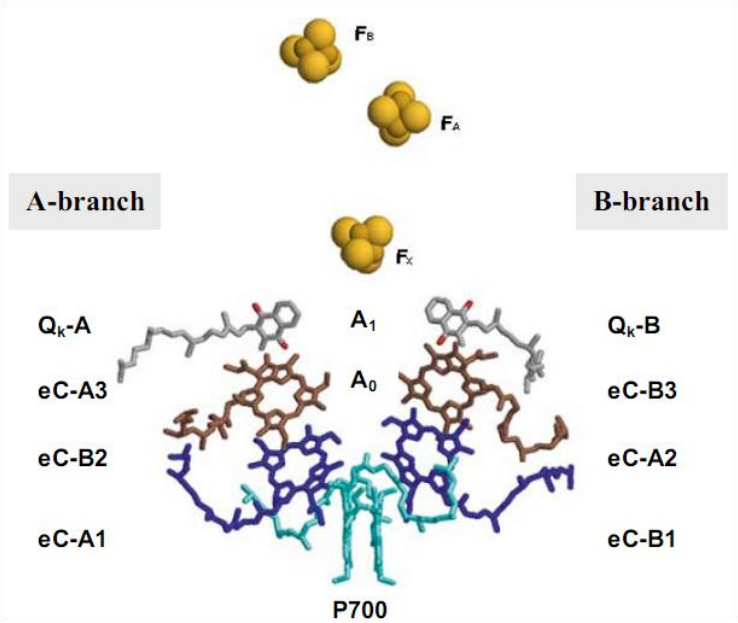

Figure 1.4 Structural arrangement of electron acceptor and donors involved in electron transfer in PSI [4]

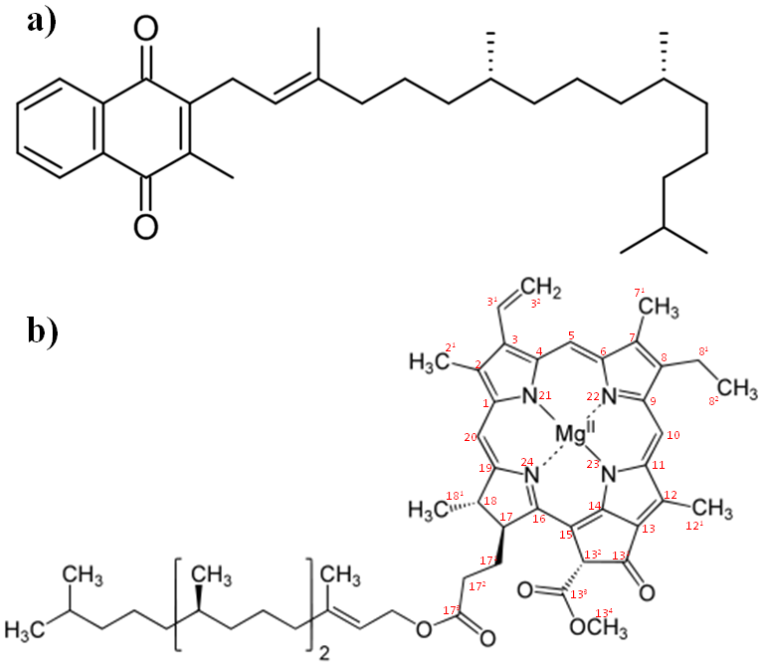

Figure 1.5 a) Chemical structure of phylloquinone (Vitamin K_1) which serves as the secondary electron acceptor at A_1 site. **b)** Chemical structure of chlorophyll-*a* molecule. Chlorophyll-*a'*, one component of the heterodimer P700, is the 13^2 epimer of chlorophyll-*a*. Chlorophyll-*a'* has a flipped project ion of 13^3 carbon from the 13^2 carbon

1.4 Electron Transfer in Photosystem I

Electron transfer in photosystem I begins when P700 receives light energy. The excitation of P700 is followed by charge separation and electron transfer through a series of co-factors of photosystem I, iron-sulfur clusters being the terminal electron acceptors. Each step of electron transfer kinetics is characterized by a specific time constant. The kinetics of electron transfer and methods of studying the electron transfer are discussed in this section.

1.4.1 Techniques and Methods for Studying Electron Transfer

A range of experimental techniques have been utilized in order to study the kinetics of electron transfer that occurs in the timescale of picoseconds to milliseconds [5]. Two widely used spectroscopic techniques in the study for the electron transfer are electron paramagnetic resonance spectroscopy (EPR) and laser flash absorption spectroscopy. EPR detects the magnetic moments of unpaired electrons of the cofactors involved in electron transfer, allowing the observation of a species directly involved in electron transfer. One disadvantage of EPR spectroscopy is its relatively low time-resolution. Laser flash absorption spectroscopy, also known as pump-probe spectroscopy or laser flash photolysis, is another common method for investigating the kinetics of electron transfer processes and is the main focus of this thesis. This technique monitors the temporal change in absorbance of a sample excited by a short, intense laser pulse. The details of the theory and applications to the study of the electron transfer processes in photosystem I reaction centers are discussed in later sections and chapters. One disadvantage to using pump-probe spectroscopy is that the optical density of the sample cannot be too high, which limits the size of the signals obtainable. One advantage of using this technique is the relatively high time-resolution and wide range of probe wavelengths that can be used.

In order to distinguish and relate the results of measurements to specific cofactors , modifications must be made to the sample. Common modifications include: lowering the temperature, introducing mutations to the sample, and pre-reducing the sample. A change in temperature changes the energetics of the electron transfer. Mutations introduced to the sample make possible the deletion or replacement of the co-factors involved in electron transfer. When co-factors are deleted the pathways in the electron transfer are inhibited. PSI with replaced co-factors may produce altered electron transfer kinetics. Pre-reduction of the sample prohibits the completion of electron transfer through the system and thus provides access to study the pathway of electron transfer. Furthermore, in pump-probe spectroscopy measurements have been done in fractioned photosystem I particles instead of whole cells. Whole cells have higher optical densities. They also scatter light considerably. These properties make pump-probe spectroscopy measurements difficult. Detergent isolated photosynthetic particles do not usually display the above types of problems. However, effects of the isolation procedure may affect to the results.

1.4.2 Kinetics of Electron Transfer in Photosystem I

The overall scheme of charge separation in wild-type PSI is illustrated in Figure 1.6 [6]. The time constants associated with the electron transfer are also shown in the figure. Excitation of the primary electron donor, P700, leads to the singlet excited state, P700*. From P700* an electron is transferred to A_0 on a picosecond timescale A_0^- transfers its electron to A_1 with a time constant of ~30 ps [7]. The charge recombination between A_0^- and $P700^+$ occurs with a time constant ~50 ns, which is slower by three orders of magnitude than the forward electron transfer process [8]. Forward electron transfer from A_1^- to F_x is characterized by two kinetic phases with time constants ~20 ns and ~200 ns [9-12]. These two phases of forward electron transfer are discussed below. When the iron sulfur clusters, F_X, F_A and F_B, are removed charge

recombination between A_1^- and $P700^+$ occurs biphasically with time constants of ~10 µs and ~100 µs [13]. In a system where F_A and F_B are pre-reduced, charge recombination between F_X^- and $P700^+$ is occurs with a time constant ~250 µs [14, 15]. Charge recombination between $F_{A/B}^-$ and $P700^+$ is characterized by a time constant of ~80 ms [5].

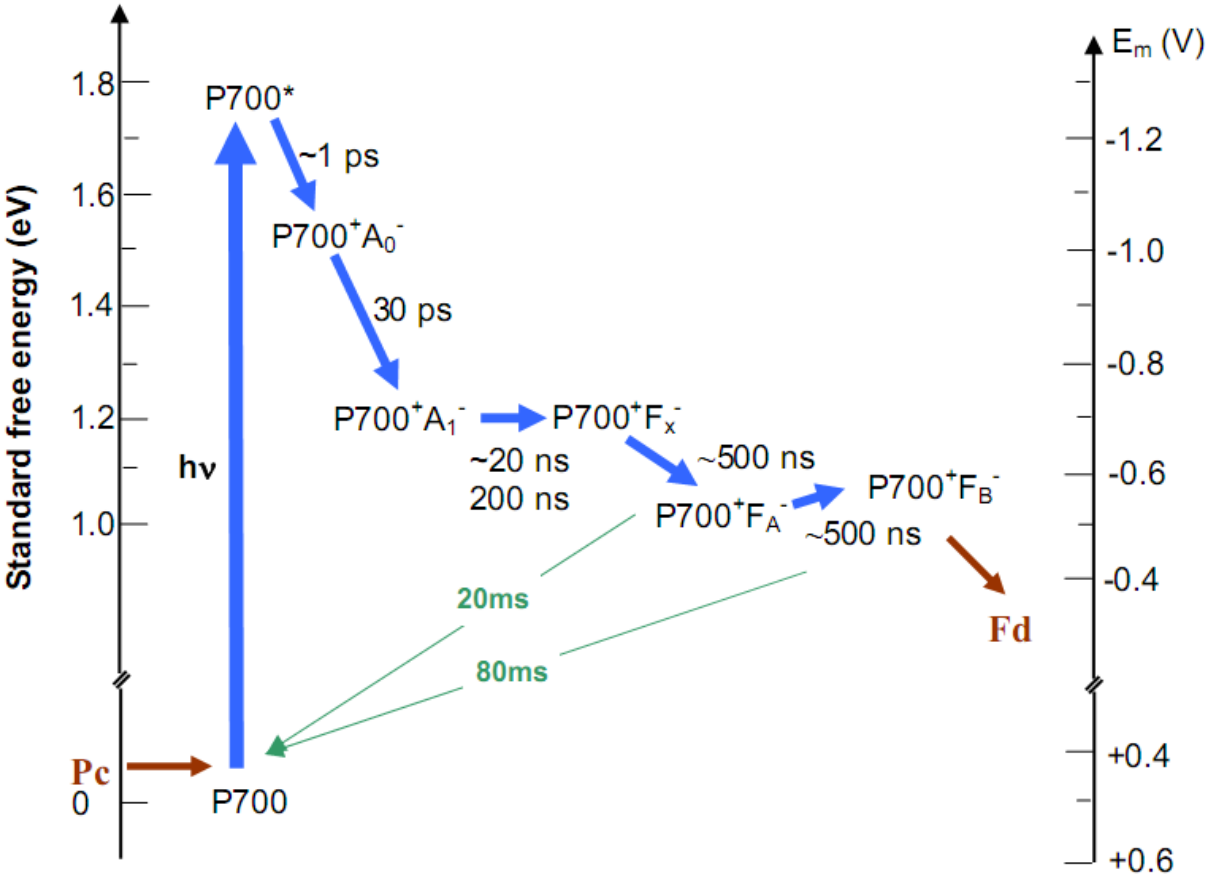

Figure 1.6 The kinetics of electron transfer in PSI [6]. The various radical pair states and the redox properties are plotted relative to the approximated standard free energies. The standard free energy of P700 was arbitrarily set to zero.

1.5 Directionality of Electron Transfer in Photosystem I

In Section 1.3 where the structure of PSI is discussed two symmetric branches of co-factors are mentioned. Furthermore, in Section 1.4.2 where the kinetics of electron transfer is discussed, two time constants of the forward electron transfer from A_1^- to F_x are mentioned [6], and it is suggested that forward electron transfer from A_1 to F_x is biphasic, occurring down both branches. The two time constants are ~20 and 200 ns, and are referred to as the "fast" phase and "slow" phase, respectively [10]. The symmetric branches and dual phases of the forward electron transfer rate raises the question of the directionality of electron transfer in PSI: whether if both PsaA-side phylloquinone and PsaB-side phylloquinone are active as a bidirectional system, or if only one of these branches participates in heterogenous but unidirectional electron transfer [16]. The currently accepted hypothesis is that the both PsaA and PsaB branches are active in electron transfer, with one branch being responsible for the fast phase and the other branch the slow phase in A_1^- to F_x forward electron transfer.

Although the exact mechanism of the biphasic kinetics has not been revealed, a number of experiments have been carried out to model the kinetics. One unidirectional model initially proposed by Setif and Brettel claims the depletion of equilibrium state between A_1 and F_x by F_A/F_B as the source of biphasic kinetics [9]. According to this model, the fast phase originates from the rapid equilibration between A_1 and F_x. The depletion of this equilibrium by electron transfer from the same A_1 to F_A/F_B gives rise to the slow phase. Since one phylloquinone gives rise to the two phases, the electron transfer is unidirectional. In contrast, one of the two models suggested by Joliot and Joliot supports the bidirectional model [17]. The experimental result by Joliot and Joliot showed that the relative amplitudes of the two phases are insensitive to the membrane potential. Two models are proposed by Joliot and Joliot from this experimental

result. One of the proposed models is the bidirectional pathway model, in which two phylloquinones, one on each branch, are oxidized by F_x at different rates. The other model suggests the unidirectional system, where a single phylloquinone gives rise to two rates by having two different conformational states. The bidirectional model, although not proven, is supported by numerous experimental results. The first experimental result to support the bidirectional model was provided by Guergova-Kuras and co-workers using site-directed mutations [18]. Site-directed mutation on green algae *Chlamydomonas reinhardtii* replaced the tryptophan that is π-stacked on phylloquinone with phenylalanine. When the mutation was introduced to the PsaA-side (PsaA-W693F), the slow phase is selectively slowed down. However, when the same mutation was made on the PsaB-side to replace the tryptophan to phenylalanine (PsaB-W673F), the faster phase is selectively slowed down. Cohen and co-workers introduced another mutation on cyanobacteria *Synechocystis* sp. PCC 6803, which replaced the axial methionine ligands of chlorophylls eC-A3 and eC-B3 to leucine [19]. The transient EPR result showed an effect on the PsaA-side mutant only, indicating that the electron transfer occurs mainly along the PsaA-side. Similarly, a mutant of *C. reinhardtii* which had a methionine ligand to chlorophyll eC-A3 (PsaA-M684H) and eC-B3 (PsaB-M664H) replaced by histidine was constructed by Fairclough and by Ramesh [20, 21]. Although the electron transfer to the PsaA-side branch was blocked, PsaA-M684H still allowed photoautotrophic growth, indicating that the PsaB-side branch was active and provided sufficient activity for photoautotrophic growth. The result from PsaA-M684H and the similar results from PsaB-M664H imply that both PsaA-side and PsaB-side branches are active in electron transport for *C. reinhardtii*. Bautista and co-workers provided another experimental support for the bidirectional electron transfer using the site-directed mutated *Synechocystis* sp. PCC6803 [10]. Two mutants,

pds$^-$ and *zds*$^-$, had their β-carotene around their phylloquinone replaced by phytoene and ζ-carotene respectively. The activity of their fast and slow phases was measured indirectly by comparing the electrochromic shift of carotenoids around the phylloquinone for wild-type and two mutants. The electrochromic shifts of the two phases are different, indicating that the carotenoid pigments serving as electrochromic markers of two phases are also different. Involvement of two different marker carotenoid pigments for two phases suggests that both PsaA-side and PsaB-side phylloquinones participate in electron transport.

1.6 Mutant Photosystem I

As some examples mentioned in the previous section illustrate, mutant photosystem I samples are widely used in the research of photosystem I electron transfer. In Section 1.5, PsaA-W693F and PsaB-W673F, which have tryptophan replaced by phenylalanine in their respective branches, PsaA-M684H and PsaB-M664H, which had methionine replaced by histidine, and *pds*$^-$ and *zds*$^-$, which had modified carotenoids around phylloquinone, were mentioned. The mutant used for the study of electron transfer involving both to and from phylloquinone is the so-called *menB* mutant of *Synechocystis* sp. PCC 6803 [22]. The *menB* gene is responsible for producing napthoate synthase, a key component in the biosynthesis of phylloquinone (Figure 1.8). A similar mutant, *menA* mutant of *Synechocystis* sp. PCC 6803, has a gene for phytyl transferase, another key component of phylloquinone biosynthesis. The initial purpose of creating the *menB* mutant was to disallow the biosynthesis of phylloquinone and produce an empty A_1 binding site, so that various quinones could then be reinserted into the vacant binding site to study the contribution of phylloquinone in the A_1 binding site. The binding site, however, was found to be occupied by a foreign quinone identified as plastoquinones-9 [22]. The presence of plastoquinones-9 in the binding site keeps the electron transfer in photosystem I active but gives

different kinetics than the kinetics of the photosystem I with phylloquinone present in the binding site. Furthermore, the low binding affinity of plastoquinones-9 makes replacement by other quinones possible [23]. Therefore the *menB* mutant is significant to the research of the kinetics of Photosystem I electron transfer as it can be studied as the subject of comparison with wild-type to investigate the contribution of phylloquinone in the binding site, or be utilized as the sample to test a variety of quinones as the plastoquinones-9 can be replaced by the other quinones due to its low affinity to the binding site.

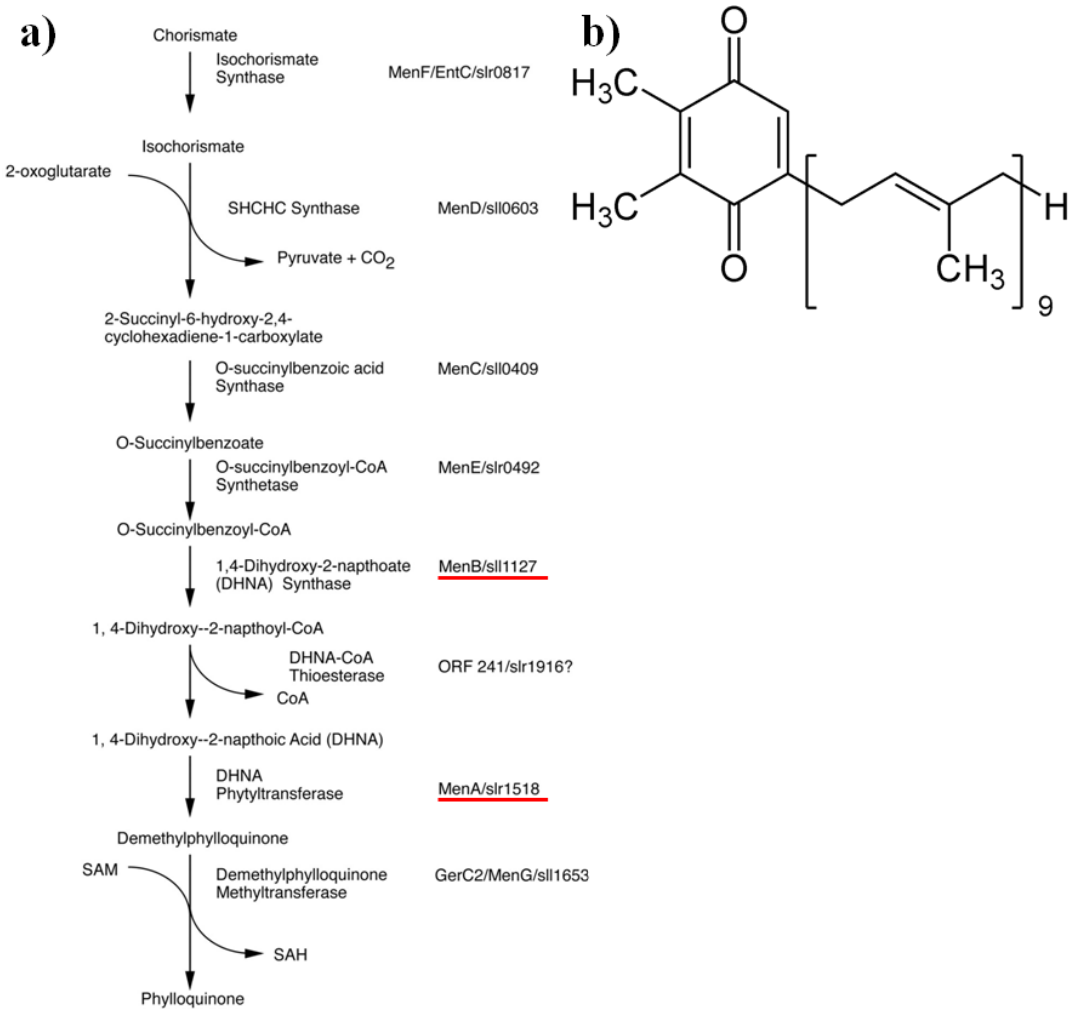

Figure 1.7 a) The biosynthetic pathway of phylloquinone [23]. In *menB* mutants, the MenB/sll1127 gene is mutated. The mutation inhibits the production of naphthoate synthase, inhibiting the production of phylloquinone. **b)** Chemical structure of plastoquinone-9.

1.7 Chlorophyll-*d* containing Photosystem I

As discussed earlier, in almost all higher plants, algae, and cyanobacteria, the light-induced electron transfer in PSI start from P700, the heterodimer of chlorophyll-*a* and chlorophyll-*a*'. In addition to this special pair, chlorophyll-*a* molecules, four more from the reaction center and ninety from the antenna pigment, make up the majority of the pigment composition of PSI. Similar to other plants, algae and cyanobacteria, cyanobacterium *Synechocystis* sp. PCC6803 and green alga *Chlamydomonas reinhardtii*, two specimens studied in this thesis for the study of PSI electron transfer, also have this chlorophyll-*a* composition in PSI. In this perspective the cyanobacterium *Acaryochloris marina*, discovered in 1996, , is an exception [24]. *A. marin*a's pigment composition in its PSI is dominated by chlorophyll-*d* molecules instead of chlorophyll-*a*. Of the chlorophyll molecules which compose *A. marina's* pigments, ≤5% are chlorophyll-*a* [24]. The difference between chlorophyll-*d* and chlorophyll-*a* is seen at R-3 position where the vinyl group in chlorophyll-*a* is replaced by the formyl group in chlorophyll-*d*.

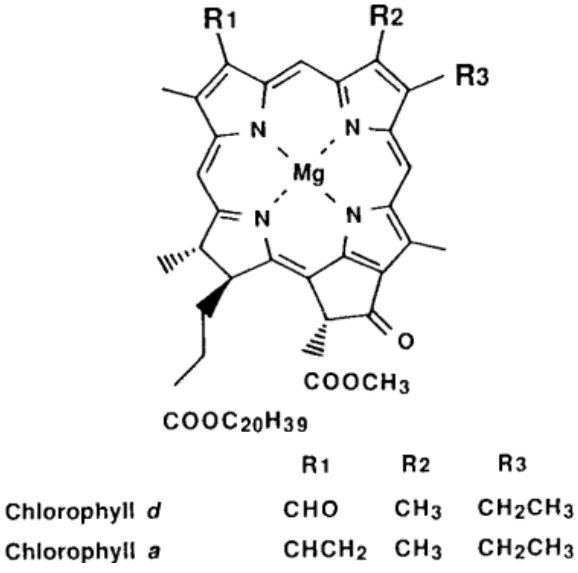

Figure 1.8 Chlorophyll-*d* molecule has a formyl group at R1 instead of a vinyl group

The other remarkable feature that distinguishes *A. marina* is that it contains α-carotene instead of β-carotene for its antenna pigment. The primary electron donor in *A. marina* is structurally similar to P700, except chlorophyll-*d* and its epimer make up the dimer. The heterodimer of chlorophyll-*d* and chlorophyll-*d'*, the 13^2 epimer of chlorophyll-*d*, is called P740. From the results of optical spectroscopic studies, the chlorophyll-*a* molecules found in *A. marina* is believed to be acting as the primary electron acceptor A_0, similar to the chlorophyll-*a* containing PSI. The secondary electron acceptor is phylloquinone, also similar to the chlorophyll-*a* containing PSI. The biphasic kinetics of the forward electron transfer from A_1 to F_X was observed through pump-probe spectroscopy on whole cells of *A. marina* at room temperature by Santabarbara and co-workers [25]. The observed lifetimes of 88 ns and 345 ns are slower than the reported rate for chlorophyll-*a* containing PSI.

2 TIME RESOLVED OPTICAL ABSORPTION SPECTROSCOPY

2.1 Laser Flash Photolysis

Flash photolysis was developed by Porter and Norrish in 1949 [26]. The technique allows the monitoring of transient species produced upon light irradiation of organic molecules, polymers, or photosynthetic units. The kinetics of transient state of a sample, which is often an excited state of a sample, exists only for a fraction of a second. Because of this excited state's short lifetime, the kinetics are generally not measurable by the absorption of fluorescence spectroscopy where measurements are made in seconds.

In order to study the absorption characteristics of excited state, a sample needs to be excited first by ground state absorption, as excited states do not occur naturally in an undisturbed sample. In laser flash photolysis, a laser pulse is used as a powerful excitation source (called pump) to generate high concentration of excited state species. The absorption characteristic of the kinetics of an excited state species generated by pump laser is monitored by the light transmitted (called probe) through the sample.

In the study of electron transfer in a photosystem, the transition states observed are reduced and oxidized states of the electron donors and acceptors. Through laser flash photolysis, kinetics of these transient species or the rate of reduction and oxidation of the electron donors and acceptors can be analyzed. These transition species, which are initially generated by a pump laser excitation, exist in the timescale range of picoseconds to tens of milliseconds. Kinetics of each transient species can be monitored by selecting a probe wavelength at which the transient species of interest absorbs.

2.2 Laser Flash Photolysis Spectrometer

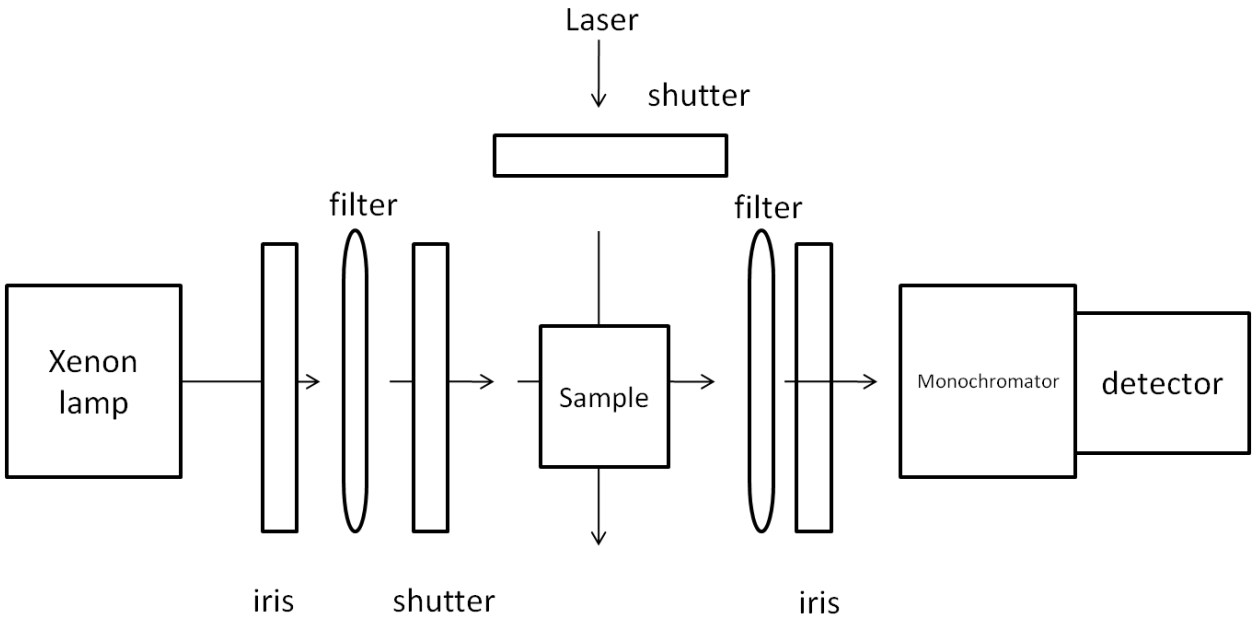

Figure 2.1 A schematic drawing of LP920 laser flash photolysis spectrometer.

The principle schematic of a laser flash photolysis spectrometer resembles the schematic of a UV-Visible range absorption spectrometer. A probe light is focused on a sample, and the transmitted light is measured by a detector. The detector converts the measured transmitted light into electrical signals that are processed by the oscilloscope. The wavelength of the probe light is selected by a monochromator that is placed either before or after the sample. In addition to this setup, a laser flash photolysis spectrometer makes a use of a pump laser. The pump laser is placed at an angle, usually 90 degrees, to the path of the probe light.

Furthermore, a pulsed flashlamp is used as a probe light source instead of a continuous light source. As in any other absorption spectroscopy, a sufficient background level is required to observe changes in transmission. In the short timescale of the laser flash photolysis measurements, a continuous light source often does not provide enough background photon flux. Therefore, a pulsed probe light source is used to increase the background photon flux

significantly, which then improves the signal to noise ratio of measurements. To protect the sample from exposure to the probe and pump source before and after the actual timescale of a measurement, shutters are placed between a sample and each light source. These shutters also make certain background measurements possible.

2.3 Optical Densities

2.3.1 Calculation of Optical Densities

The change in probe light transmittance through the sample over time is measured by the detector and processed as electrical signals by the oscilloscope, which can then be analyzed as the change in absorption. The change in absorption of the sample before, during, and after the pump excitation is calculated in units of change in optical density, ΔOD. ΔOD, expressed in terms of the intensity of transmitted light, is:

$$\Delta OD(t,\lambda) = \log\frac{I_b}{I_T(t,\lambda)}$$

where I_b is the intensity of the transmitted light before the pump excitation, and I_T is the intensity of the light on and after excitation. The Beer-Lambert law relates optical density with the sample concentration, path length that light travels, and the extinction coefficient of the sample as:

$$OD = \varepsilon cd$$

$$\varepsilon: extinction\ coefficient$$

$$c: sample\ concentration$$

$$d: path\ length$$

Then, the general expression of ΔOD for laser flash photolysis measurement can also be summarized as:

$$\Delta OD(t,\lambda) = \varepsilon_T(\lambda)c_T(t)d - \varepsilon_G(\lambda)c_T(t)d - \phi(\lambda)c_G(t)$$

where ε_G and ε_T are the extinction coefficients of the ground state species and the transient state species respectively. c_T and c_s are the sample concentration of the transient species and the ground state species, and ϕ is fluorescence spectrum of the sample. In the region of wavelengths where ground state sample does not absorb, and assuming no fluorescence, ΔOD is

$$\Delta OD = \varepsilon_T(\lambda)c_T(t)d$$

indicating that ΔOD is positive. If the measurement is taken in the region where ground state absorbs more dominantly instead, ΔOD shows the same decay kinetics but negatively:

$$\Delta OD = -\varepsilon_G(\lambda)c_T(t)d$$

2.3.2 Calculation of Background Correction

Often times, depending on the environment of the experiment, including a sample; probe and pump stability; probe and pump wavelengths; and the timescale of a measurement, background corrections need to be taken into account for the ΔOD calculation. Two of the corrections that can be included in the calculation are probe background correction and fluorescence correction.

Probe background correction is measured in order to correct for probe pulse fluctuations (Figure 2.1). The probe pulse intensity may fluctuate within the monitored time window depending upon the timescale of the measurement, width of the pulse, and the position on the pulse monitored. To compensate for the fluctuations in the probe, a measurement is taken without the pulse excitation in addition to the regular measurement. The calculation of ΔOD with the probe background correction is expressed as:

$$\Delta OD(t) = \log\frac{I_b^T}{I_b^{PB}} + \log\frac{I_{PB}(t)}{I_T(t)}$$

where $I_T(t)$ is the intensity of probe light transmitted through the sample over time in the

presence of a laser flash, and $I_{PB}(t)$ is the intensity of the probe background over time. The first term of the function is expressed with I_b^T and I_b^{PB}, which are the constant background levels of the transmitted light and probe background respectively before the timing of the pump excitation in the absence of the pump pulse.

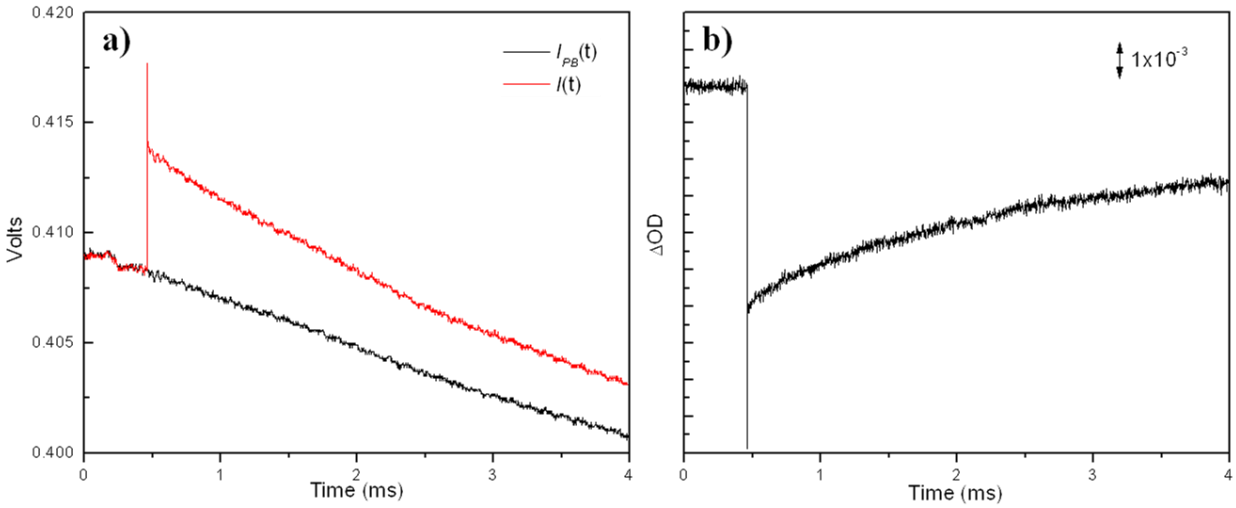

Figure 2.2 a) Raw data consists of transient (*red*) and probe background (*black*).
b) Calculated ΔOD from the transient and probe background in **a)**. Even when the pulse profile is not stable, probe background can take into account the fluctuations.

Fluorescence Background correction is measured to offset a contribution from sample fluorescence, scattered laser light, and laser noise (Figure 2.2). The background is measured by recording the signal from the signal of the pump-excited sample while having the probe beam blocked by the probe shutter. The calculation of ΔOD with the fluorescent background correction is expressed as:

$$\Delta OD(t) = \log\left(\frac{I_b}{I_T(t) - I_F(t)}\right)$$

where $I_F(t)$ is the intensity of the fluorescent background, and I_b and $I_T(t)$ are the intensity of the constant background level of the transmitted light before the excitation and the intensity of the transmitted light over time before and after the excitation respectively.

Furthermore, both the probe and fluorescence background corrections can be applied together (Figure 2.3). In such a case, the function for the calculation of the optical density is:

$$\Delta OD(t) = \log \frac{I_b^T}{I_b^{PB}} + \log\left(\frac{I_{PB}(t)}{I_T(t) - I_F(t)}\right)$$

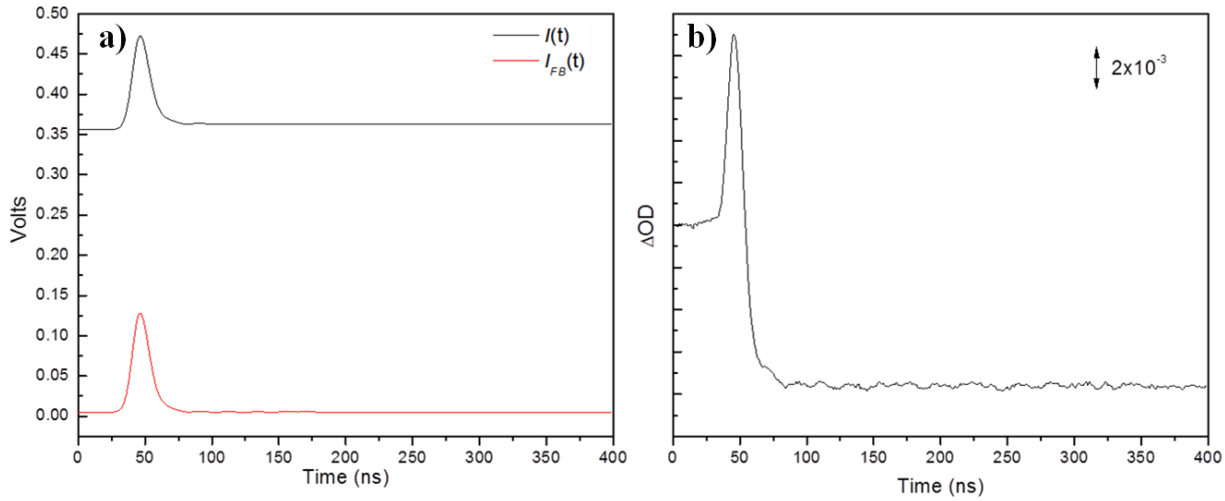

Figure 2.3 a) Raw data consists of transient (*black*) and fluorescent background (*red*). **b)** Calculated ΔOD from the transient and fluorescent background in **a)**. Peaks observed in raw data, both in transient and fluorescent background, are the contributions by fluorescence.

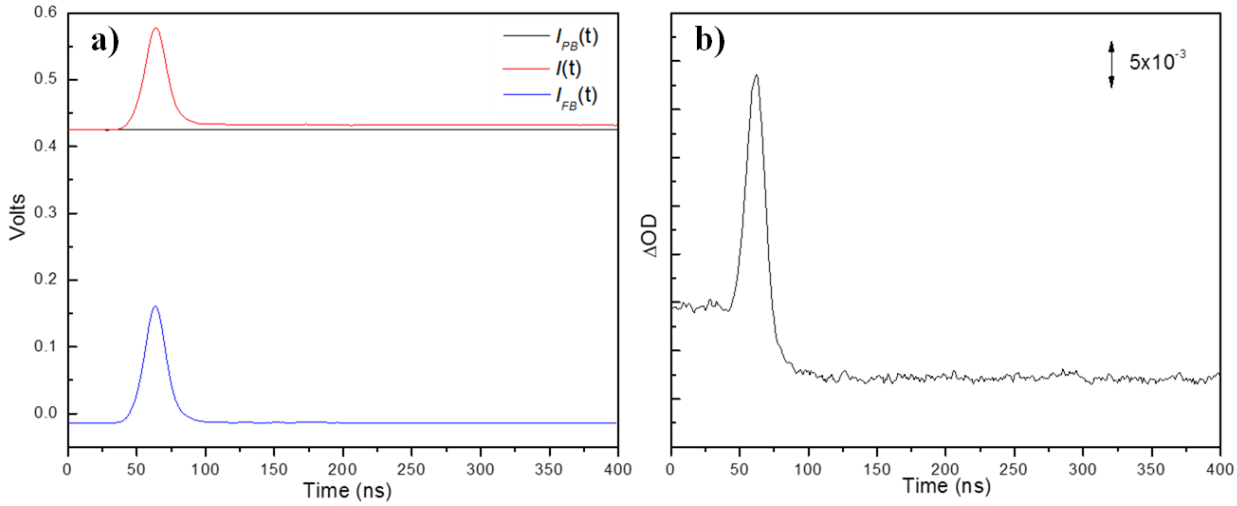

Figure 2.4 a) Raw data consists of transient (*red*), probe background (*black*), and fluorescent background (*blue*). **b)** Calculated $\boldsymbol{\Delta OD}$ from the transient with fluorescent and probe background subtracted. Both the fluorescent contributions and the probe pulse drift are taken in account by having both backgrounds subtracted in calculation of$\boldsymbol{\Delta OD}$. The disadvantage is the reduced signal-to-noise ratio.

2.4 Decay Laws Associated with Molecular Kinetics

From the ΔOD observed over time, the information of kinetics of transition states can be extracted. Specifically, the lifetime of kinetics and an order of the decay process can be determined. The lifetime of kinetics that is calculated from the ΔOD observed over time is the mean lifetime, the time at which the population of interest is reduced to $1/e \approx 0.3678$. In the previous chapter, the time constants of electron transfer in photosystem I describes the half-life, the time at which the population of the interest is reduced to one half. The relationship between the mean lifetime and half-life can be expressed as:

$$t_{1/2} = \tau \ln 2$$

In the next section, the decay laws associated to molecular kinetics, specifically electron transfer, are discussed.

2.4.1 First Order Decays

A first order decay depends on the concentration of only one species. In a case of laser flash photolysis, the species could be an electronically excited molecule or a molecule in triplet state in an absence of a quencher. More specifically, in the study of Photosystem I kinetics, reduced or oxidized cofactors go through the first order decay in forward electron transfers or in charge recombination reactions. Thus, the only decay law that this thesis focuses on is the first order decay.

In the first order decay, the reaction rate *r* with respect to a concentration of decaying species *M* is

$$r = -\frac{d}{dt}[M] = k[M]$$

where *k* is the first order decay constant. This reaction rate can be re-written as

$$\ln[M] = \ln[M_0] - kt$$

$[M_0]$ is the initial concentration of *M*. Furthermore, the equation can be expressed as

$$[M] = [M_0]e^{-kt}$$

Since, in laser flash photolysis, the concentration of the sample is directly related to the ΔOD due to Beer-Lambert Law, the above equation in terms of ΔOD is

$$\Delta OD(t) = \Delta OD_0 e^{-kt}$$

The mean lifetime τ and the decay constant is inversely related

$$\tau = \frac{1}{k}$$

Thus the mean lifetime of the first order decay can be calculated from the exponential fits of the observed ΔOD as a function of time.

2.4.2 Pseudo-first Order Decays

In a situation where a transient species is being quenched by a second species, such as in a case where a triplet state is being quenched by molecular oxygen, an enhanced rate of decay relative to unimolecular decay is observed. The reaction rate is then expressed as

$$r = -\frac{d}{dt}[M] = k_1[M] + k_q[M][Q]$$

where *M* is the transient species and *Q* is the second species quenching *M*. Usually, the concentration of the quenching species is much greater than that of the quenched transient species. The rate constant can now be expressed as

$$k_2 = k_1 + k_q[Q]$$

which suggests that the observed rate constant k_2 is greater than k_1, meaning a faster decay time compared to the first order decay.

2.4.3 Second Order Decays

A second order decay depends on the concentration of the two first order species. An example of a reaction that goes through a second order decay is triplet-triplet annihilation. An equation of this reaction can be written as

$$[M] + [M] \overset{k_q}{\rightarrow} products$$

The rate equation of such a reaction is

$$-\frac{d}{dt}[M] = k_1[M] + k_a[M]^2$$

which gives, in terms of ΔOD,

$$\Delta OD(t) = \frac{\Delta OD_0}{(1 + k_2 t)} e^{-k_1 t}$$

$$k_2 = \Delta OD\ k_a$$

The decay is not exponential. The initial part of the decay is characterized by fast non-exponential decay, while the final part is characterized by exponential decay.

2.5 Pump-Probe Spectroscopy on Photosystem I Kinetics

The application of laser flash photolysis, or pump-probe spectroscopy, on Photosystem I has revealed much of the kinetics of electron transfer. For the laser flash photolysis experiments, the sample used are usually whole cells or fractionated PSI particles prepared from the specimens. Some common specimens, for both whole cells and PSI particles, are cyanobacterium *Synechocystis* sp. PCC 6803, green alga *Chlamydomonas reinhardtii*, and spinach leaves [6, 9, 11]. The sample is usually suspended in a buffer such as Tris·HCl at ~ pH 8.0 containing *n*–dodecyl *β*-D-maltoside, a detergent to reduce PSI aggregation [4, 22]. Glycerol is included in this buffer when the measurement is done at a low temperature [12]. Additional

reagents such as sodium ascorbate, phenazine methosulfate (PMS), methyl viologen, and dichlorophenolindophenol (DCPIP) are added depending on the experiments [4, 27].

To determine the lifetime of the electron transfer, time-dependent absorbance changes of the co-factor of the interest needs to be measured over time. Therefore the wavelength of the probe light needs to be selected so that the difference in absorbance between the ground state and the transient state of the measured co-factor is considerably large. Absorption difference spectra, on which the difference in absorbance between certain time intervals measured at variety of wavelengths are plotted, relays this information.

387 nm is assigned as the maximum wavelength for the changes in the phylloquinone absorbance. The maximum wavelength is determined from the phyllosemiquinone-minus-phylloquinonne difference spectrum in the solution [11]. In 1988 Brettel performed pump-probe spectroscopy measurement on PSI particles prepared from cyanobacteria *Synechococus* sp. at 387 nm at room temperature. The half-life obtained from the observed decay was $t_{1/2} \approx 200$ ns. The difference spectrum of the 200 ns phase was then constructed for the wavelengths between 330 nm and 500 nm at room temperature. The fast phase was not observed in this experiment. In 1993, Brettel and Setif conducted another pump-probe spectroscopy experiment on PSI particles at room temperature [9]. The particles were prepared from spinach and *Synechocystis* sp. PCC 6803. In this experiment, two phases that correspond to the forward electron transfer from the phylloquinone to their iron-sulfur cluster were observed. The half-lives of the fast and slow phases at room temperature were $t_{1/2} \approx 15$ ns and $t_{1/2} \approx 150$ ns. Agalarov and Brettel, in 2003, investigated the temperature dependence of these two phases on monomeric PSI particles from *Synechocystis* sp. PCC 6803 [12]. At room temperature, the lifetimes of the two phases were determined as $\tau = 14$ ns and $\tau = 340$ ns. These lifetimes, converted to half-life time

constants, are $t_{1/2}$ = 9.7 ns and $t_{1/2}$ = 235 ns respectively. The slow phase slowed upon cooling while the fast phase stayed independent of temperature change.

In the blue region of the difference spectrum of A_1/A_1^-, an absorbance decrease at ~450 nm and an absorbance increase at ~487 nm also exist. These peaks are assigned to the electrochromic band shifts of carotenoid pigments around phylloquinone in A_1. Because the electrochromic shifts accompany A_1 reduction, the wavelength in this region can be used to probe the electron transfer in A_1. Bautista and co-workers performed pump-probe spectroscopy experiments on PSI at 380 – 390nm and 480 nm [10]. The measurements were done on particle PSI and whole cells of *Synechocystis* sp. PCC 6803. Both the fast and slow phases were observed for particle PSI and whole cells. The averaged half-lives of particle PSI analyzed at 380 – 390 nm were $t_{1/2}$ = 8 ns and $t_{1/2}$ = 177 ns, while the half-lives observed at 480 nm were 9 ns and 152 ns. The measurement at 480 nm on whole cells decayed with half-lives $t_{1/2}$ = 8 ns and $t_{1/2}$ = 180 ns. Another kind of the electrochromic shift is observed between 680 nm and 702 nm. At these wavelengths, the electrochromic band shift of the chlorophyll-*a* pigments in the vicinity of A_1 is seen. Dashdorj and co-workers obtained the half-life time constant of 300 ± 50 ns for the slow phase through these wavelengths for particle PSI from *Synechocystis* sp. PCC 6803 [28].

One of the kinetics commonly measured by the pump-probe spectroscopy other than the forward electron transfer from A_1 to iron-sulfur cluster is the $P700^+$ charge recombination kinetics [6]. The $P700^+$ charge recombination kinetics can be measured at around 703 nm, the wavelength where the absorbance peak of P700 is, or at beyond 750 nm, where P700 no longer absorbs but $P700^+$ starts absorbing. The back reaction of $P700^+$ with a reduced iron-sulfur cluster

is reported to have lifetime of ~80 – 100 ms [6]. Shinkarev and co-workers obtained 107 ms for a particle PSI from *Synechocystis* sp. PCC 6803 measured at 832 nm [4].

Although the complete mechanisms of the kinetics of the electron transfer in the *menB* mutant has not been revealed yet, certain paths of electron transfer have been studied more extensively. Two paths of the *menB* mutant electron transfer that have time constants confirmed are the forward electron transfer from A_1 and the $P700^+$ charge recombination kinetics. Semenov and co-workers determined in 2000 that the fast and slow phases of the A_1 forward electron transfer rate are τ = ~15 μs and τ = ~250 μs at 315 nm and 485 nm [22]. The $P700^+$ charge recombination kinetics was studied by Shinkarev at 832 nm, and the lifetime of τ = 2 ms was resultant [4].

The summary of the observed time constants are listed in the table below (Table 2.1). All the constants are in terms of mean-lifetime. Those that are initially reported as half-lives are converted to mean-lifetime.

Table 2.1 A summary of some of the reported time constants. All the constants are the mean-lifetime. The lifetimes of two phases of the forward electron transfer from A_1 and the $P700^+$ charge recombination kinetics are reported. The state of the PSI, whether particle or whole cells, are also noted.

Reported by:	PS I	Fast phase	Slow Phase	$P700^+$ recombination
Brettel (1988) [11]	*Synechocystis* sp. PCC6803 particle	-	289 ns	-
Brettel and Setif (1993) [9]	Spinach *Synechocystis* sp. PCC 6803 particle	22 ns	216 ns.	-
Agalarov and Brettel (2003) [12]	*Synechocystis* sp. PCC 6803 Particle (monomeric)	13.6 ns	339 ns	-
Bautista (2005) [10]	*Synechocystis* sp. PCC 6803 Particle	11 ns 13 ns	255 ns 219 ns	-
Bautista (2005) [10]	*Synechocystis* sp. PCC 6803 Whole cells	12 ns	260 ns	-
Dashdorj (2004) [28]	*Synechocystis* sp. PCC 6803 particle	-	432 ± 72 ns	-
Shinkarev (2002) [4]	*Synechocystis* sp. PCC 6803 particle	-	-	154 ms
Semenov (2000) [22]	*menB* mutant particle	15 µs	250 µs	2 ms

3 EXPERIMENTAL DETAILS

3.1 Pump-Probe Spectrometer

The standard setup of the laser flash photolysis spectrometer, along with modifications we introduced, are discussed in this section. In all work reported here an LP920 Edinburgh Instruments pump-probe spectrometer was used[29]. An overview of the setup of the LP920 is shown in Figures 3.1 and3.2). The setup includes a probe light source, a pulser unit, a spectrometer controller system, a monochromator, a photomultiplier detector, an oscilloscope and a laser light source. The pulsed probe light is directed through the sample. The laser light is also directed through the sample, perpendicular to the probe light. The probe light after traversing the sample is then focused on the monochromator, where the wavelength of the light is selected, and then focused onto a photomultiplier tube detector. The signal detected by the photomultiplier tube is processed by an oscilloscope. The timing and synchronization of the pump and probe light pulses, the laser firing, and the opening and closing of the mechanical shutters are all manipulated by the spectrometer control unit via a software interface.

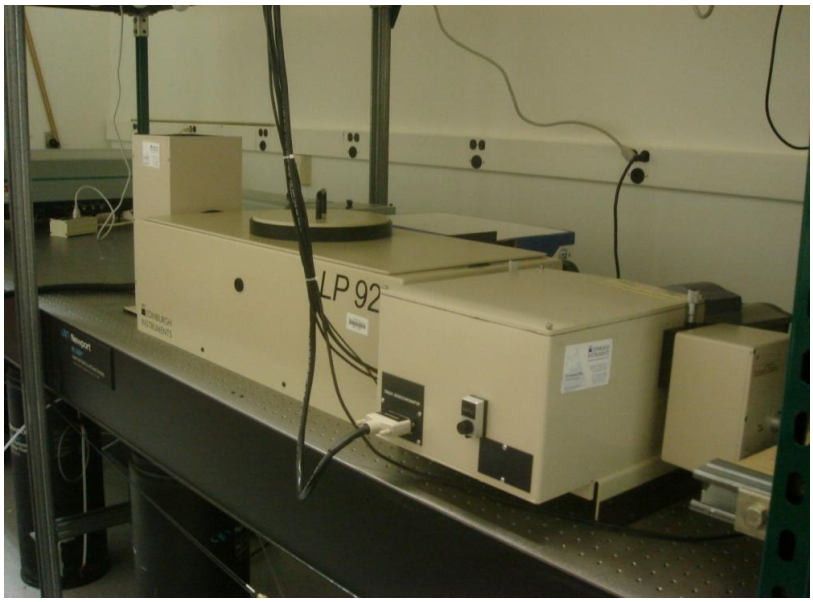

Figure 3.1 LP920 laser flash photolysis spectrometer.

3.1.1 Probe Light Source

The probe light source used in the LP920 is a 450 W xenon flash lamp. The flash lamp produces a continuous spectrum in the 190-2600 nm range [29]. The lamp's current, in the range of 10 to 27 A, can be set from the front panel of the lamp's power supply. The lamp is enclosed in a rigid aluminium housing which helps limit electromagnetic interference from the lamp source. The housing also includes a spherical reflector behind the lamp. The positions of the lamp and the reflector can be adjusted independently horizontalyl and vertically.

A pulser unit, discussed in next section, allows the lamp to be used in pulsed mode with the frequency up to 10Hz.

3.1.2 Pulser Unit

The pulser unit, xP920, works in combination with the probe light source Xe920 to produce short period and high current probe pulses. As discussed earlier, the probe pulse is crucial in increasing the background photon flux to improve a signal-to-noise ratio in short timescale measurements. The pulse has a fast rising and falling time, giving it a rectangular shape. The size of this rectangular pulse can be adjusted from 0.2 to 10 ms in width, and 50 to 300 A in current. The repetition rate of the pulse is 10Hz at the fastest. The lamp power, P, is determined as a product of the current (I), pulse width (T), repetition rate (f), and the lamp voltage (set at factory setting 60 and not adjustable by the user) during pulsing. The expression of the lamp power, therefore, is

$$P = 60 \times I \times T \times f$$

and the maximum power output is set as 300 W [29].

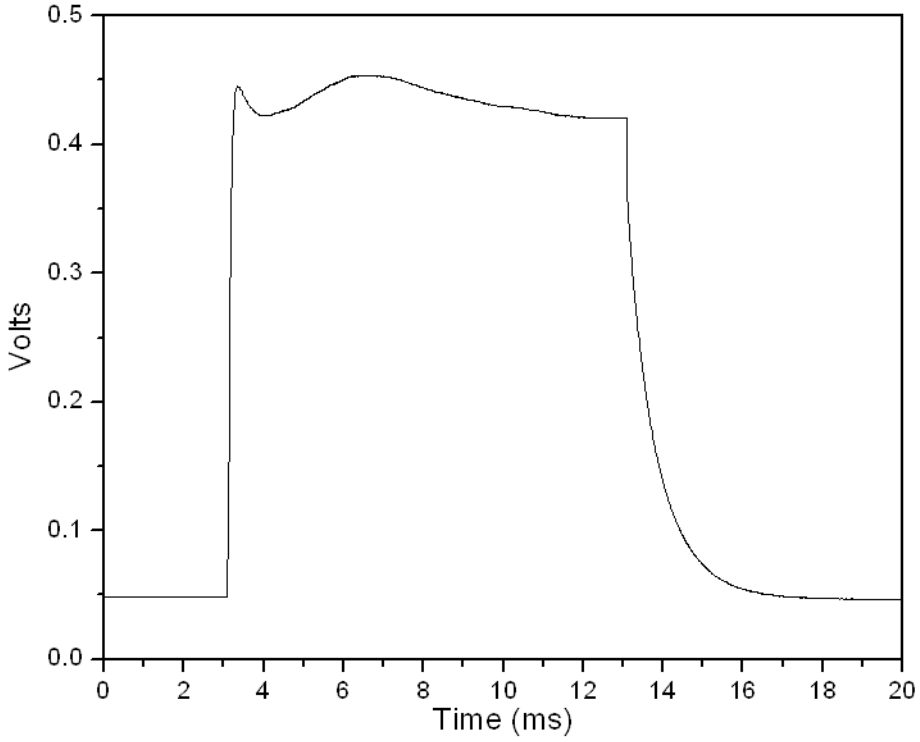

Figure 3.2 A typical optical pulse profile of xenon flashlamp, Xe920, pulsed by the pulser unit XP920. The pulse in this figure is set to be 10 ms in width and is fired at 16 Hz. The trace is an average of 160 measurements. In an actual measurement of kinetics, a position of the pulse with the least drift in the specified time range is chosen as the time window of the measurement. In addition to the repetition rate, width (duration) of the pulse, height (voltage) of the pulse can directly be adjusted by changing current.

3.1.3 Spectrometer Controller

The LP920 controller serves as the central timing unit for the spectrometer. Through the software interface, the controller provides access to the settings of the probe pulse, pump laser, probe and laser shutters, and the monochromator positioning. In addition, the oscilloscope trigger and supply voltage to the detector are also processed by the controller unit.

3.1.4 Monochromator

A Czerny-Turner monochromator, manufactured by Bentham Instruments (model TMc300), with symmetrical spherical mirrors is placed between a sample chamber and a photomultiplier detector. The monochromator is comprised of two symmetric spherical mirrors and a plane reflection grating. Wavelength selection through grating angle adjustment is automated by a software controlled micro-step motor. The reflection grating has 1800 grooves per millimeter, blazed at 500 nm. The region of wavelength coverage is from 200 nm to 900 nm. The motorized grating covers this region of wavelength in minimum step size of 0.05 nm. At both the entrance and the exit of the monochromator are the microscrew apertures that control the slit size to determine the spectral bandwidth.

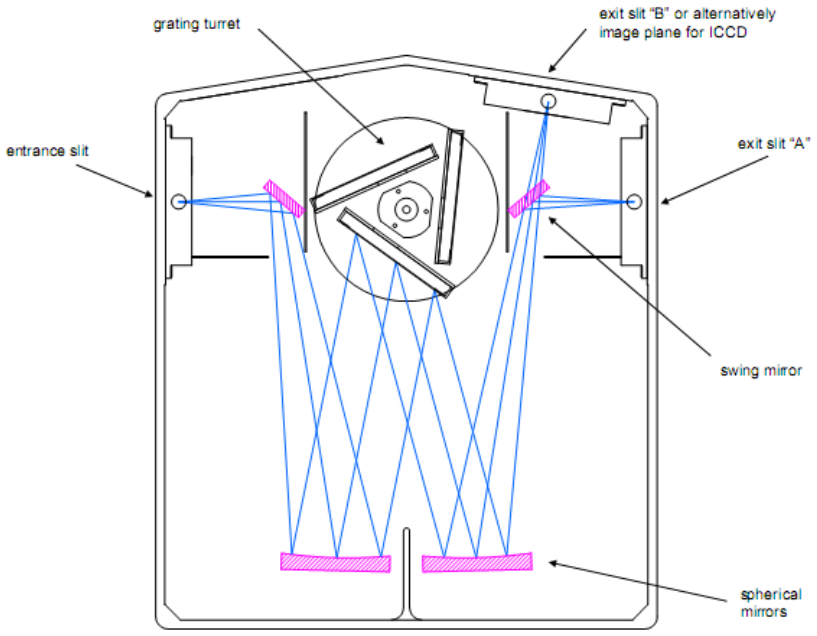

Figure 3.3 A schematic drawing of a monochromator TMc300. Taken from reference [29].

3.1.5 Photomultiplier Detector

A red sensitive photomultiplier tube, Hamamatsu R928, is incorporated in the detector assembly. The photomultiplier tube covers a region of wavelength from 187 nm to 900 nm, with peak sensitivity at 400nm. The detector assembly uses an interlock shutter that protects the photomultiplier tube. A bias voltage can be controlled by a turning knob on the detector assembly. The detector has two versions of the amplifier circuit: fast amplifier and slow amplifier. The fast amplifier circuit has a rise time of less than 1 ns for an output impedance of 50 Ω, and is suitable for measurements in timescale up to 100 μs [29]. The slow amplifier design with an impedance of 1 MΩ is chosen for measurements in timescale longer than 100 μs.

3.1.6 Oscilloscope

The oscilloscope used in this set up is the Tektronix TDS3012B digital storage oscilloscope. The signal from a photomultiplier detector is digitally recorded on the oscilloscope. The oscilloscope is connected to the computer by an Ethernet connection for fast data transfer and thus accessible by the spectrometer software.

3.1.7 Sample Compartment

The sample compartment is a light tight box where a sample is placed (Figure 3.5). The lid that provides access to the interior of the box is equipped with microswitches that trigger the photomultiplier detector's interlock shutter.

A sample holder is placed inside the sample compartment (Figure 3.5). While the cross beam geometry where the probe light and pump laser intersect on the sample perpendicularly is used in the regular setup, the holder is capable of providing other configurations such as quasi co-linear geometry and diffuse reflectance geometry. In quasi co-linear geometry, the probe and the laser are crossed at a small angle, increasing the cross section on the sample. In diffuse

reflectance geometry, the probe light is reflected off samples in powder, bulk, or non-transparent film form at an angle. The pump laser is focused on the sample surface where the probe light is reflected. In all configurations, fixed apertures can be set on both sides of the sample to restrict the size of the probe light.

Protecting the sample in sample holder from the two light sources are the electronic shutters. In addition to providing protection from photo-bleaching and photo-degradation due to prolonged exposure to the probe or pump sources, the shutters also control the timing and the length of the exposure. The shutters can set to be fully open, fully closed, or timed via the spectrometer software. Both shutters are synchronized and the duration of their opening can also be controlled by the software.

Two focusing lenses are placed in line with the course of the probe light. One lens is positioned by the xenon lamp unit and the other lens is located by the entrance of the monochromator. The lens by the xenon lamp unit focuses the probe light source from the lamp unit on to the sample. The lens by the entrance of the monochromator, along with the mirror optics inside the monochromator, re-focuses the light on the photomultiplier detector. The focusing lenses are coupled to the manual irises, which are mainly used for light attenuation.

Figure 3.4 A sample compartment and a sample holder.

3.1.8 Laser

The laser used as a pump source for the system is Continuum Surelite I-10. The Q-switched Nd:YAG laser produces a 4 – 6 ns pulse at 532 nm with max energy of 200 mJ. The repetition rate of the flashlamp is set to 10 Hz.

3.1.9 Software

All of the components of LP920 are accessed and operated by the software by Edinburgh Instruments: L900. L900 provides a platform to access each component to modify its settings, run various kinds of measurements, and analyze collected data. Specifically, the hardware that can be accessed through L900 are: the pump laser system, probe light system, oscilloscope, and detector.

In pump laser setting, the flashlamp properties, Q-switch properties, and repetition rate can be modified. The flashlamp trigger delay can be changed to shift the flashlamp trigger in respect to the pulsed xenon lamp. The delay controls the position of the laser pulse relative to

the xenon lamp pulse; Q-switch trigger delay, on the other hand, is responsible for the interval between the timing between flashlamp trigger and Q-switch trigger, and alters the energy intensity of the laser pulse. For the probe light setting, pulse width, pulse current, and pulse shutter width can be adjusted within the limit of maximum power. Photomultiplier impedance can be set as either 50 Ω or 1 MΩ depending on the timescale of the measurement. 1 MΩ is recommended for a measurement longer than 100 μs, and 50 Ω is used for a measurement faster than 100 μs.

For the measurement set up the timescale of the measurement, number of measurement, types of background to use, and mode of probe light can be specified. The timescale of the measurement, or duration of acquisition, can be varied from a hundreds of nanosecond range to a hundreds of millisecond range. The background to be subtracted, as explained earlier, can be selected from either no background, probe background subtracted, fluorescence background subtracted, or both probe and fluorescence background subtracted.

The obtained measurement can be fitted to find the mean lifetime on L900, or converted to text files which can then be analyzed on other graphing software.

3.2 Investigated Samples

The PSI complexes studied in this thesis are fractionated particles. PSI particles were isolated from cyanobacterium *Synechocystis* sp. PCC 6803. The particles of *menB* mutant PSI were also constructed and isolated from *Synechocystis* sp. PCC 6803. Both the wild-type PSI and *menB* mutant PSI particles were suspended in a Tris buffer (25 mM, pH 8.3) with a 0.04 % β-DM. The sample was placed in a 1 x 0.5 cm plastic cuvette. The probe light beam passed through a 1 cm side of the cuvette. The reaction medium, in addition to the Tris buffer, contained sodium ascorbate, DCPIP, and PMS.

PSI particles from *Chlamydomonas reinhardtii* were also studied. The buffer and the composition of the reaction medium were the same as the ones for PSI particles from *Synechocystis* sp. PCC 6803. The sample was also measured in a 1 x 0.5 cm plastic cuvette.

Isolated particles of chlorophyll-*d* containing PSI from *Acaryochloris marina* were studied briefly with the same buffer and the reaction medium as the ones used for chlorophyll-*a* containing PSI.

All the PSI samples were frozen until re-suspension by the Tris buffer, and the measurements were made at room temperature (294K).

4 SAMPLE ABSORPTION SPECTRA

Absorption spectroscopy in the 400-800 nm region was used to initially characterize the PSI particles studied. Absorption spectra of PSI particles from wild-type and *menB* mutants of *Synechocystis* sp. PCC 6803, *Chlamydomonas* (*C.*) *reinhardtii*, and *Acaryochloris* (*A.*) *marina* (all re-suspended in a 25 mM Tris buffer at pH 8.3 with 0.04% β-DM)in the 400-800 nm range are shown in Figures 4.1 and 4.2. Absorption measurements were made using a Shimadzu UV-1601 spectrometer. The spectra shown in figures 4.1 and 4.2 were normalized to the Q_y peaks in a red region, at 680 nm for the wild-type (WT) and *menB* mutant PSI particles from *Synechocystis* sp. PCC 6803 (S6803), 678 nm for *C. reinhardtii*, and 703 nm for *A. marina*.

Although the Q_y peak positions were the same for both WT and *menB* mutant PSI (680 nm), the two spectra exhibit significant differences around ~498 nm (Figure 4.1). This difference in absorption around 500 nm between WT and menB PSI was also reported in a recent study [30]. The exact cause of the increase in the absorbance in near 500 nm in menB PSI has not been determined, but it is likely associated with a differing amount of carotenoids in the mutant PSI particles. This observation is of some relevance because the 450-500 nm region is widely studied in pump-probe spectroscopy of PSI particles, primarily because it is thought that electrochromic band-shifts of carotenoid pigments occur in this region (see below). *A.marina* PSI particles also display increased absorption in the 450-550 nm region, compared to that for PSI particles from *C. reinhardtii* or *S. 6803.* Although there is no reason why the carotenoid content in *A. marina* PSI should resemble that of *C. reinhardtii* PSI.

In all of the studies reported here we have used laser flashes at 532 nm (green light) to excite the samples. As can be seen in figures 4.1 and 4.2, the sample absorption at 532 nm is close to 0.25 (neglecting scattering) in optical density (OD) units for all samples.

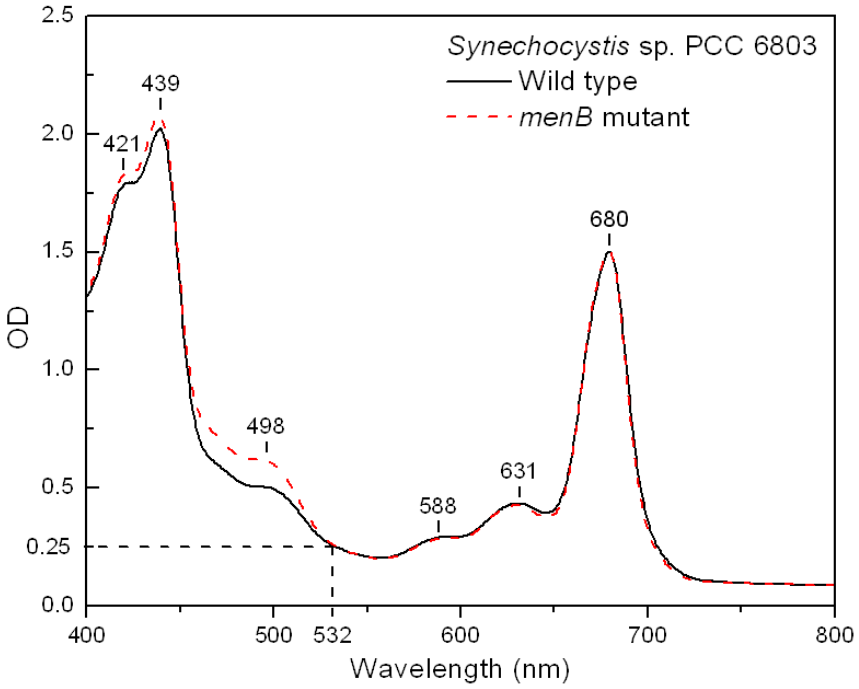

Figure 4.1 Absorption spectra of wild type (*black*) and *menB* mutant PSI (*red*) particles from *Synechocystis* sp. PCC 6803.The spectra were normalized to an OD = 1.5 at 680 nm.

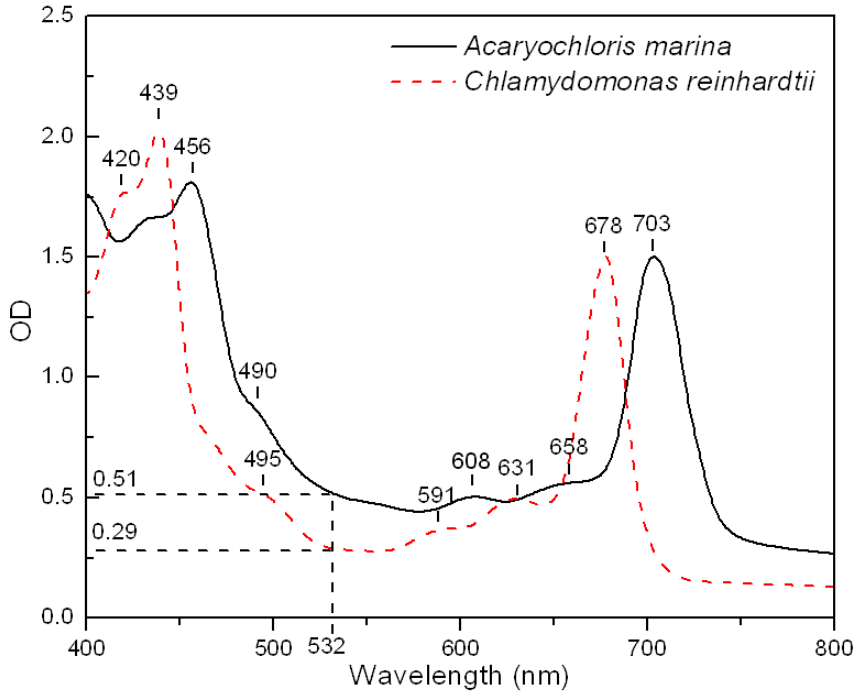

Figure 4.2 Averaged absorption spectrum of wild-type PSI particles from *Acaryochloris marina* (*black*) and *Chlamydomonas reinhardtii* (*red*) normalized to OD = 1.5 at 703 nm and 678 nm respectively.

5 CHARGE RECOMBINATION IN WT AND *MENB* MUTANT PSI PROBED AT 703 NM.

For both WT and *menB* mutant PSI flash induced absorption changes were monitored using the LP920 pump-probe spectroscopy system. The sample cuvette was 1 x 0.5 cm, and was oriented in the sample compartment so that the probe light beam had a path length of 1 cm. The kinetics associated with charge recombination were probed at 703 nm, following laser excitation at 532 nm. The laser excitation repetition rate was set to 0.37 Hz and the data shown are the result of multiple laser flashes. The intensity of the probe light as a function of time without laser flash excitation was also monitored (called a probe background signal) and subtracted from the signals obtained with laser flash excitation. This is necessary because the probe intensity temporal profile is not perfectly "flat".

For *menB* PSI, measurements were made on 10 µs, 100 µs, 400 µs, 1 ms, 4 ms, and 10 ms time scales. For WT PS I, measurements were made in 10 µs, 100 µs, and 4 ms time scales. For the measurements made on time scale shorter than 100 µs, the impedance of the detector was set at 50 Ω. For the measurements in a longer time scale, the detector had 1 MΩ impedance. All measurements in this chapter were undertaken at a probe wavelength of 703 nm. The probe beam wavelength was selected by two 700 nm interference filters. One filter was placed before the sample, and one filter was placed after the sample, in front of the entrance slit of the monochromator. The monochromator was set to transmit at 703 nm.

WT and menB PSI samples were suspended in 25 mM Tris, pH 8.3 with 0.04 % β-DM, 20mM sodium ascorbate, and 10 µM DCPIP. All samples had an optical density of 1.5-1.65 at 680 nm.

Measurements at a probe wavelength of 703 nm obtained using WT PSI particles, on the 10 μs, 100 μs, and 4 ms timescales, are shown in Figure 5.1a, b and c, respectively. The negative signal that appears within the instrumental time resolution upon 532 nm laser excitation of the sample shows no decay on the 10 μs and 100 μs timescales. There is a small absorption recovery (~20%) observed on the 4 ms timescale (Figure 5.1c). The data on the 4 ms timescale in Figure 5.1c is well fitted by a single exponential function with lifetime $\tau = 1.09 \pm 0.02$ ms.

The ~1 ms decay is due to $P700^{+}F_{x}^{-}$ recombination that occurs in a portion of reaction centers that are nonfunctional in electron transfer to $F_{A/B}$, or have lost $F_{A/B}$ [31, 32]. Most of the (negative) signal in Figure 5.1c does not decay on a 4 ms timescale. It is well known that $P700^{+}F_{A/B}^{-}$ decays in ~30-80 ms in intact PSI particles [31, 32] So a likely conclusion is that the non-decaying component in figure 5.1c is due to that $P700^{+}F_{A/B}^{-}$.

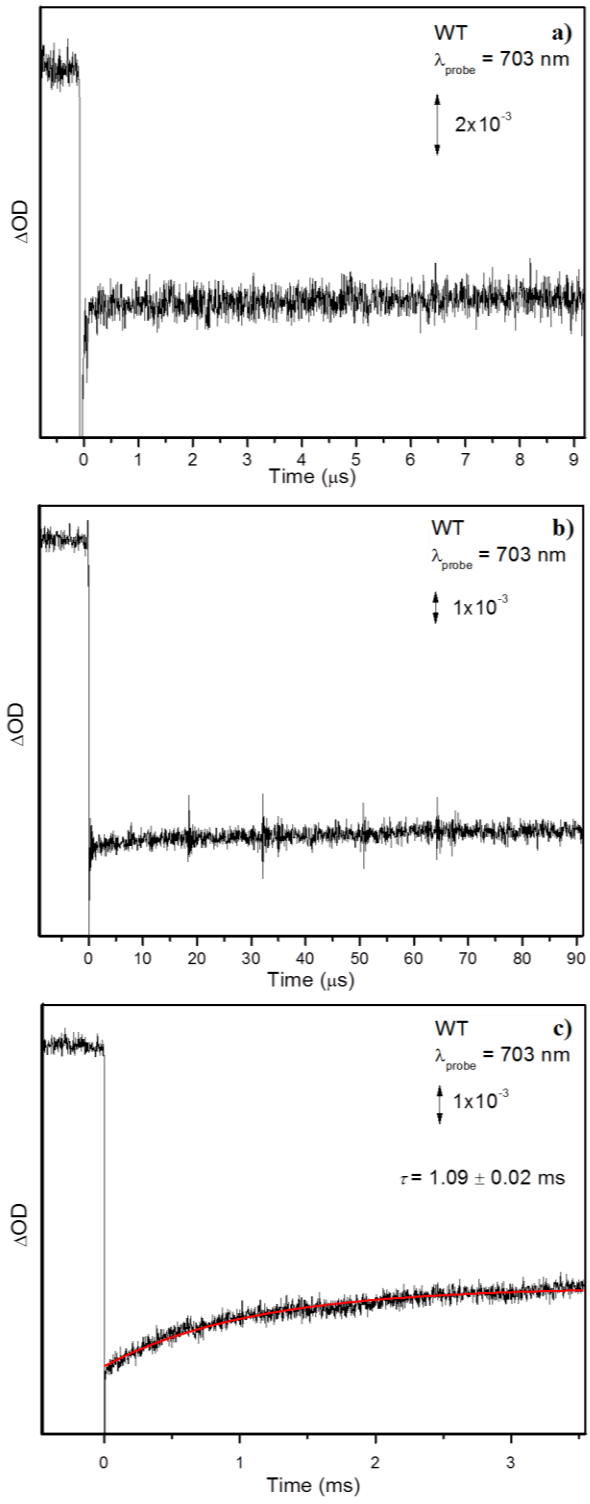

Figure 5.1 Absorption changes at 703 nm, following 532 nm excitation of WT PSI particles. Absorption changes were probed on **a)** 10 μs, **b)** 100 μs, and **c)** 4 ms time scales. The trace in **c)** was fitted by a single exponential function, the result of the fitting is shown (*red*). The data shown in **b)** and **c)** are averages of multiple sets of 640 measurements. The trace in **a)** is the average of 640 measurements.

Absorption changes at 703 nm in *menB* PSI on six different timescales (10 µs, 100 µs, 400 µs, 1 ms, 4 ms, and 10 ms) are shown in Figure 5.2. The trace in each figure is fit using a single exponential function. The calculated fitted curve, along with the residuals (which give a measure of how well the fitted curve simulates the data), are also shown in the figures. The data in Figure 5.2f is well fit by a single exponential with lifetime of 3.29 ± 0.10 ms. Over 70 % of the original signal amplitude decays with a 3.29 ms lifetime. A 3.29 ms time constant is in agreement with that found in previous work [16]. The lifetimes obtained from fitting the data in Figure 5.2 are summarized in a Table 5.1.

The data on six time scales are mutually normalized and plotted together on a logarithmic time scale in Figure 5.3. The log scale helps highlight the amplitude of each kinetic phase. The plot shown in Figure 5.3 is very similar to that found previously for *menB* PS I particles probed at 832 nm [4].

Plots of the residuals in Figure 5.2 show that a single exponential fit poorly describes the data in some cases. In such cases, a faster decay phase of small amplitude is present. These faster decay phases, seen in measurements on 10 µs and 100 µs timescales, are discussed in depth in the next chapter.

Although a variety of time constants were obtained, the lifetimes outlined in Table 5.1 indicate two ranges of time constants, between 3–16 µs and 2–3.3 ms. The 3.3 ms decay phase, as discussed earlier, is due to charge recombination between $P700^+$ and $F_{A/B}^-$. This decay is more than an order of magnitude shorter than for the corresponding process in WT PSI particles. The 2–16 µs decay phase has small amplitude and resembles the 4.1 µs time constant reported previously [4].

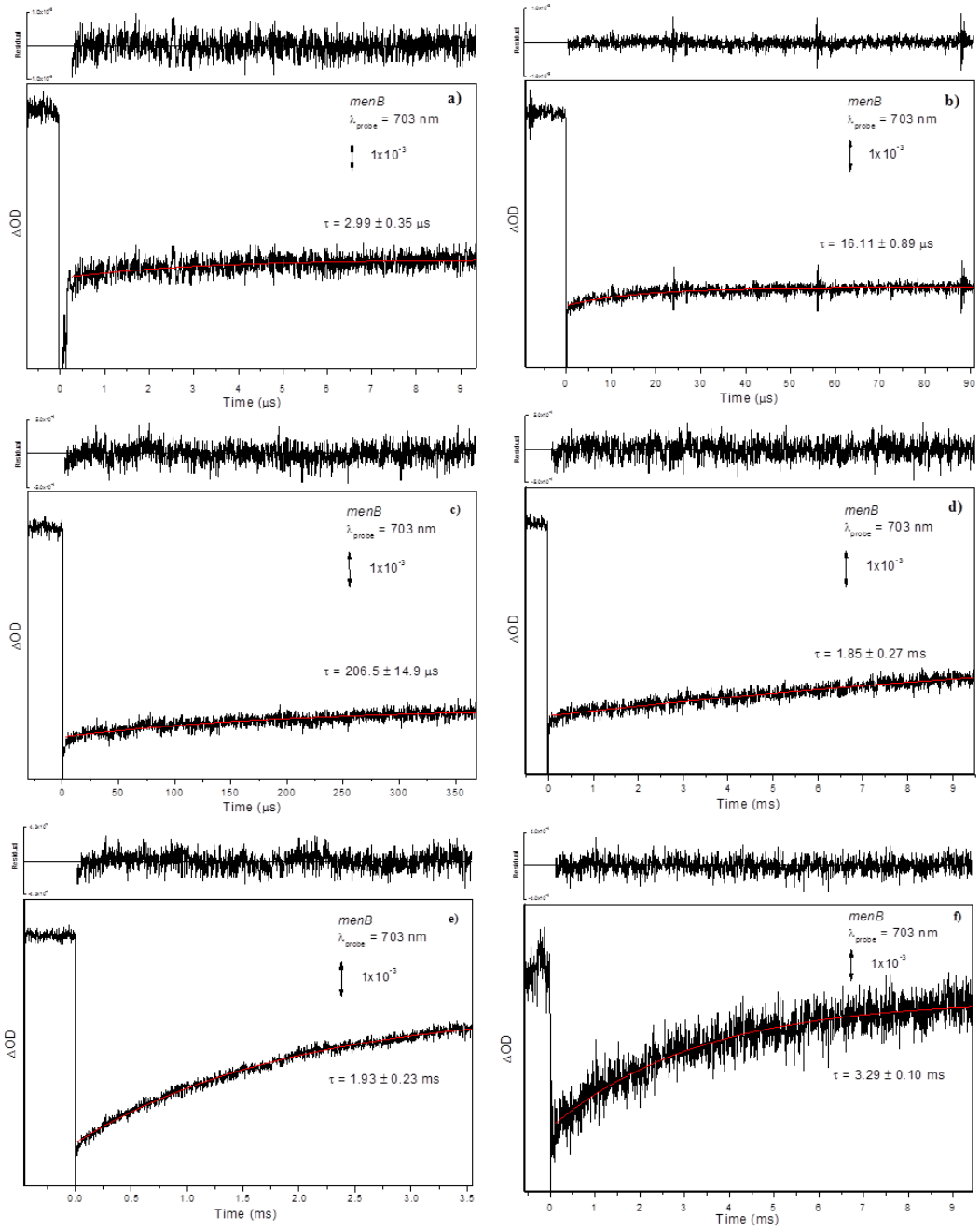

Figure 5.2 Absorption changes at 703 nm on six different timescales following 532 nm laser excitation of *menB* PSI particles. Single exponential fits to the data are the smooth lines shown in red. Listed time constants are also shown. For the traces on the 100 µs, 400 µs and 1 ms, time scales 640 measurements were averaged. For measurements on the 10 ms timescale 340 measurements were averaged. The traces in 10 µs, and 4 ms are averages of multiple sets of 640 measurements.

Table 5.1 Summary of calculated lifetimes obtained by fitting the kinetic data at 703 nm for *menB* PSI particles. The kinetics are associated with $P700^+$ charge recombination.

Time scale	Lifetime (τ)
10 µs	2.99 ± 0.35 µs
100 µs	16.11 ± 0.89 µs
400 µs	206.5 ± 14.9 µs
1 ms	1.85 ± 0.27 ms
4 ms	1.93 ± 0.23 ms
10 ms	3.29 ± 0.10 ms

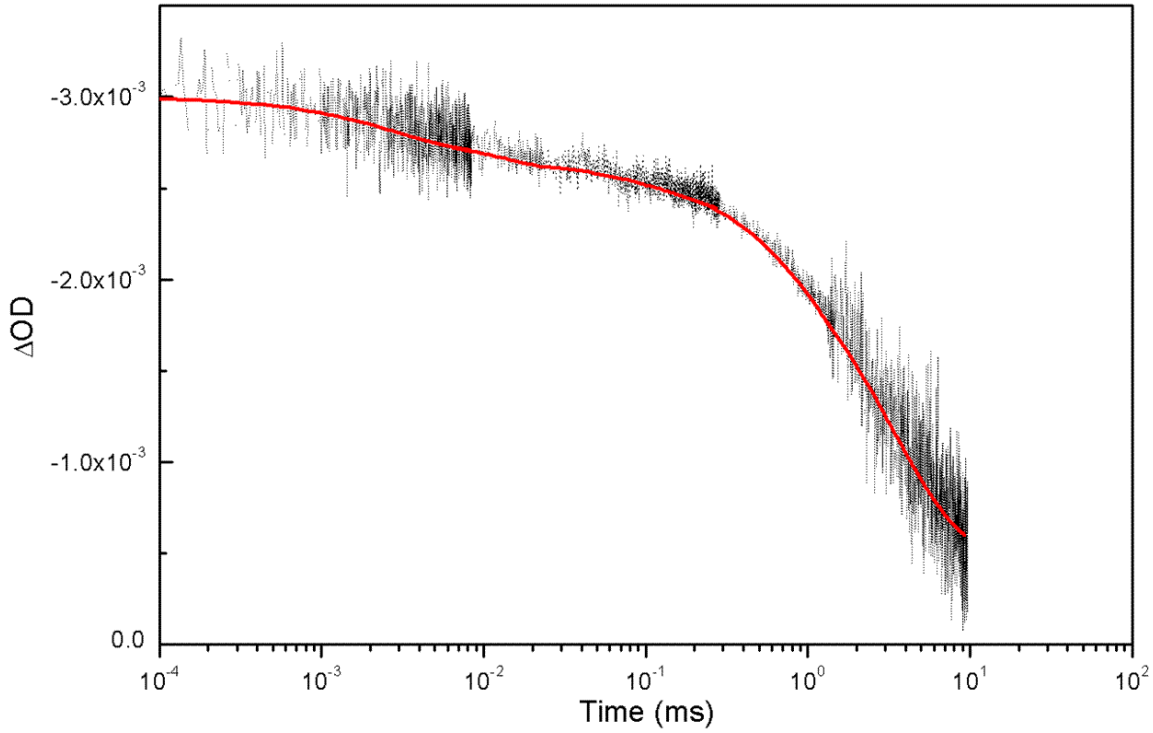

Figure 5.3 Semi logarithmic plot of normalized transient absorption data taken from measurements at 703 nm on six timescales (as shown in Figure 5.2). Data were normalized to an initial ΔOD = -3.0×10^{-3}**.**

6 NANOSECOND ABSORPTION CHANGES TO DISTINGUISH WT AND *MENB* MUTANT PSI PARTICLES.

To further investigate light induced processes occurring in WT and *menB* mutant PSI, measurements were made on a 400 ns time scale, probing at 800 and 703 nm. The main reason behind this measurement is to better resolve the decay phase seen in the first microsecond after flash excitation of PSI samples (Figure 5.2a).

The LP920 pump-probe spectrometer set up is identical to that described in the previous chapter. To probe at 800 nm, an 800 nm interference filter was placed in front of the sample, and a 572 nm long pass filter was placed after the sample, in front of the entrance slit of the monochromator, in order to block scattered 532 nm light from the pump laser. The monochromator was set to transmit light at 800 nm. Both the fluorescent and probe backgrounds were subtracted from each measurement. All data presented in this chapter are averages of multiple sets of 640 measurements (laser flashes).

In the previous chapter, the reaction medium for WT and *menB* PSI contained 25 mM Tris buffer with 0.04% β-DM at pH 8.3, 20mM sodium ascorbate, and 10 μM DCPIP. Phenazine methosulfate (PMS) is commonly used to rapidly re-reduce $P700^+$ [27]. This is useful in experiments when $P700^+$ is very long lived. The time scale for PMS to fully re-reduce $P700^+$ is concentration dependent. In our measurements 10 μM PMS is added to the previously described reaction medium. Measurements on a 400 ns timescale for both WT and *menB* PSI, were undertaken at 703 and 800 nm, in the presence of PMS. These data were compared to measurements made in the absence of PMS. The optical density for each PSI sample is adjusted to 1.6 at 680 nm for all measurements in this chapter.

Figure 6.1 shows flash induced absorption changes at 703 nm, for WT and *menB* PSI on a 400 ns timescale, in the absence of PMS.

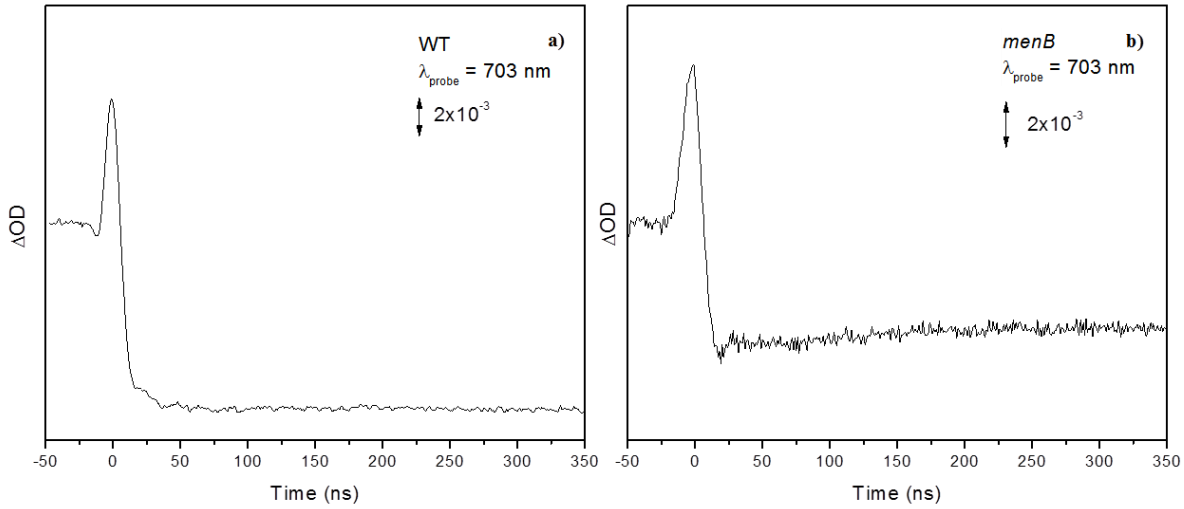

Figure 6.1 Flash induced absorption changes at 703 nm in **a)** WT and **b)** *menB* PSI, in the absence of PMS.

At 703 nm, the *menB* PSI absorption changes differ from that of WT PSI, in both signal size and decay kinetics. Although the fluorescent backgrounds have been subtracted in both measurements, fluorescence that could not be eliminated is seen as a spike near t = 0 ns. These fluorescent spikes are ignored in assessing the signal amplitude and decay kinetics below. The initial flash induced absorption change for WT PSI is approximately -9.0×10^{-3}, while for *menB* PSI it is -6.0×10^{-3}. For WT PSI the absorption change does not evolve (is constant) over the whole 400 ns time window. On the other hand, for *menB* PSI, a small amplitude decay phase is observed (Figure 6.1b). This decay phase has an amplitude that is close to the noise level in the experiment, and therefore its significance is relatively minor. The signal amplitude may be smaller in *menB* PSI due to the A_1 binding site not being fully occupied by plastoquinone-9, or not all incorporated plastoquinone-9 is functional in electron transfer.

Figure 6.2 compares flash induced absorption changes for WT and *menB* PSI at 800 nm, in the absence of PMS.

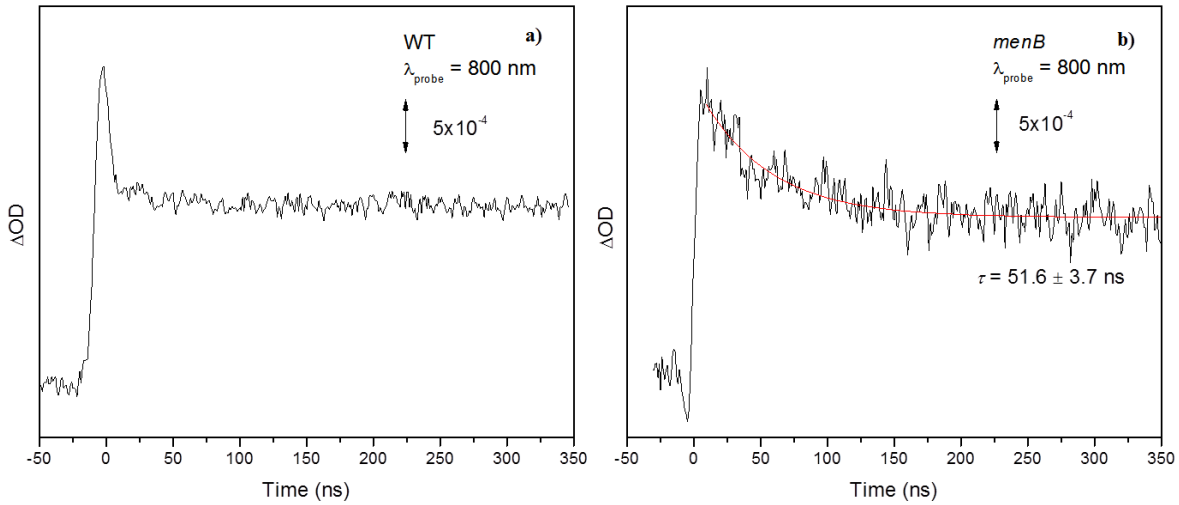

Figure 6.2 Flash induced absorption changes at 800 nm in **a)** WT and **b)** *menB* PSI, in the absence of PMS. The data in **b)** is fit to a single exponential decay with lifetime of 51.6 ns.

At 800 nm, no decay phase is observed for WT PSI. For *menB* PSI, however, a distinct 52 ns decay phase is observed. WT and *menB* PSI are easily distinguishable at 800 nm. For *menB* PSI the signal intensity decays to approximately half its initial amplitude (Figure 6.2b). When a data in figure 6.2b was fit to a single exponential, excluding the region corresponding to a fluorescent spike (15-20 ns), a similar lifetime was obtained.

There are two characteristics features that can be used to differentiate *menB* PSI from WT PSI. First, for *menB* PSI the signal intensity is ~30% smaller than that for WT PSI at 703 nm. In contrast, at 800 nm, the intensities are similar. Second, a 52 ns decay phase is observed at 800 nm for *menB* PSI, but not for WT PSI. These features are discussed below.

Figure 6.3 shows flash induced absorption changes at 703 nm for (a) WT PSI and (b) *menB* PSI in the presence of PMS.

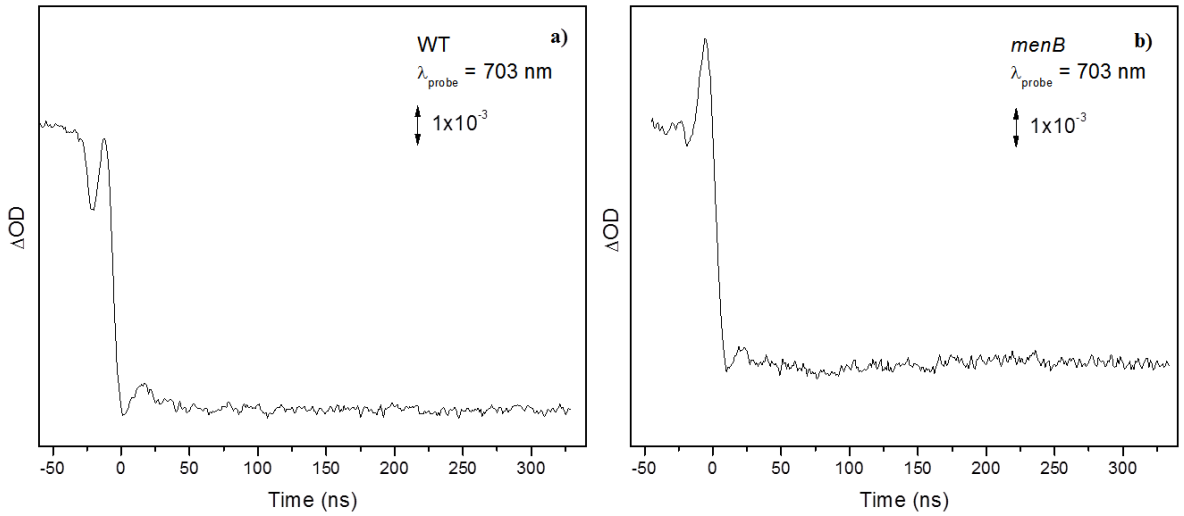

Figure 6.3 Flash induced absorption changes at 703 nm in **a)** WT and **b)** *menB* PSI, in the presence of PMS.

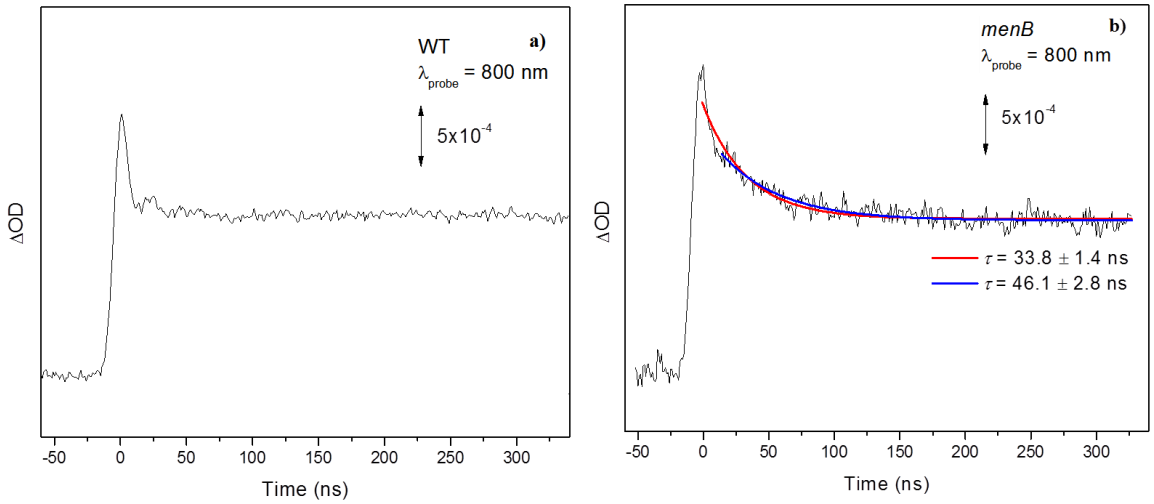

Figure 6.4 Flash induced absorption changes at 800 nm in **a)** WT and **b)** *menB* PSI, in the presence of PMS. Two single exponential fits (*red*, *blue*) are shown in **b)** and differ only on where the fitting starts (0 or 15 ns). In either case a time constant of 34-46 ns is calculated.

Comparing figures 6.1a and 6.3a it can be concluded that the addition of PMS does not greatly alter the flash induced absorption changes at 703 nm for WT PSI. The same could also be said for the flash induced absorption changes at 703 nm for *menB* PSI.

Figure 6.4 shows flash induced absorption changes at 800 nm for (a) WT PSI and (b) *menB* PSI, in the presence of PMS.

For both WT and menB PSI the data in the absence and presence of PMS are similar at both 703 and 800 nm. The data in figure 6.4d was fitted to a single exponential component. There appears to be an observable fluorescent spike in the data in figure 6.4d, which complicates the fitting procedure. Figure 6.4d therefore shows two different single exponential curve fits, starting at either 0 or 15 ns. In both cases a lifetime of 33.8 - 46.1 ns is calculated. This is very similar to that found in measurements in the absence of PMS (Figure 6.2b). Again, an ~ 50 ns decay phase is observed at 800 nm upon excitation of *menB* PSI particles, but not for WT PSI particles.

As discussed above, the fluorescent background subtraction failed to cancel out all the fluorescence or laser scattering artefacts that contribute to the data. Therefore, 10 – 15 ns after the peak of the initial spike cannot be used as a reliable indicator of the kinetics in PSI.

Addition of PMS to the reaction medium seems to have no significant effect on the decay phases on a 400 ns timescale in either WT or *menB* PSI. For WT PSI, at both 703 nm and 800 nm, after the initial spike, the absorption changes remain constant over the first 400 ns. The ~50 ns decay at 800 nm for *menB* PSI, has an amplitude that is roughly half of the initial peak intensity. After the ~50 ns decay process is complete the signal amplitude (at 800 nm) remaining is close to that found for WT PSI at 800 nm. Fluorescence or laser scattering artefacts obscure any kinetic phases that may contribute during the first 15-20 ns following laser excitation. It is possible that the lack of any decay phase at 800 nm in WT PSI is because the putative decay rate is within this 15-20 ns time window.

The origin of the ~50 ns decay phase at 800 nm in *menB* PSI is not known at present. As the absorbance change at 800 nm corresponds to the change in $P700^+$ population, the decay signifies a fast decrease in $P700^+$ population. The 50 ns decay could result from triplet state ($P700^T$) formation. $P700^T$ displays positive absorption at 800 nm [33]. However, if the extinction coefficient is smaller for $P700^T$ than for $P700^+$, then an absorption decrease would be expected upon $P700^T$ formation. The extinction coefficients at 820 nm are 5500 $M^{-1}cm^{-1}$ for $P700^T$ and 7010 $M^{-1}cm^{-1}$ for $P700^+$ [15, 34]. Such extinction coefficients are in line with our triplet state formation hypothesis. In further support of our hypothesis, $P700^T$ formation is well known to occur in 20-250 ns, depending on the species used and on the sample conditions [8]. In the PSII RC, triplet Chl_T is formed directly from the $P_{680}{}^+Phe^-$ radical pair recombination with a time constant of 57 ns, a rate similar to our observed ~50 ns decay in *menB* PSI [35].

If $P700^T$ forms in 50 ns then it should decay in 1-500 μs [15, 33, 36]. Such a decay should be obvious at both 703nm and 800 nm. Also, if $P700^T$ forms in 50 ns, then this formation would not be obvious in the absorption changes at 703 nm, which are due primarily to the loss of ground state absorption of P700. Although the decay of $P700^T$ should be obvious at 703 nm, such changes are not entirely clear in the transient data at 703 nm for *menB* PSI, although small decays with lifetimes of ~3 μs and 207 μs are observed in Figure 5.2a and 5.2c, respectively.

If $P700^T$ formation is observable at 800 nm the so should the $P700^T$ decay be observable at 800 nm. Figure 6.5 compares flash induced absorption changes for WT (a) and *menB* (b) PSI at 800 nm on a 200 μs timescale. For WT PSI no absorption changes are observable at 800 nm (Figure 6.5a). For *menB* PSI absorption changes are clearly present. Fitting the data in Figure 6.5b to a double exponential function yields time constants of 8.5 and 60 μs. We hypothesize that the 8.5 μs time constant observed at 800 nm, and possibly the 3 μs time constant at 703 nm

(Figure 5.2a) is associated with the decay of $P700^T$. In support of this hypothesis it has been shown previously in PSI under highly reducing conditions that $P700^T$ decays in ~10 μs [15, 36].

$P700^T$ usually forms by recombination of $P700^+A_0^-$. If this is the case then a likely conclusion would be that either the A_1 binding site is empty, or that plastoquinone in the binding site is somehow non-functional, in a portion of the *menB* PSI particles.

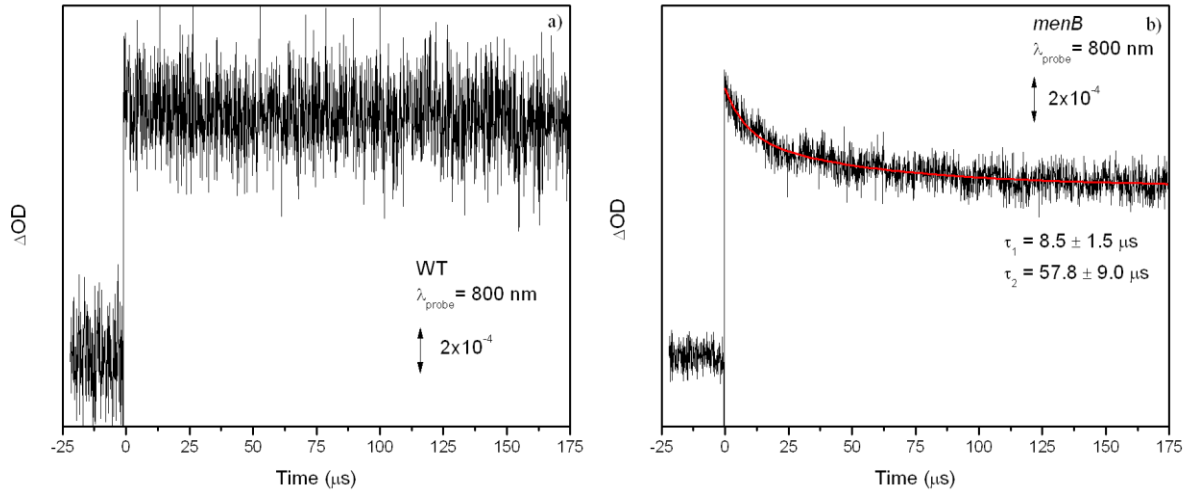

Figure 6.5 Flash induced absorption changes at 800 nm in **a)** WT and **b)** *menB* PSI on a 200 μs timescale. By fitting the data to a double exponential function time constants of 8.5 and 57.8 μs are calculated for *menB* PSI (*red* in **b)**).

Electron transfer from A_1^- to F_x slows down considerably in *menB* PSI, from exhibits ~20 ns and ~250 ns in WT PSI to ~20 μs and ~250 μs in *menB* PSI [9, 10, 22]. The longer lifetime of A_1^- in *menB* PSI will likely lead to an increased instance of charge recombination from the $P700^+A_1^-$ state, leading to $P700^T$ formation. In WT PSI with F_X, F_A and F_B pre-reduced, electron transfer from A_1^- to F_x is inhibited, and $P700^+A_1^-$ recombines by forming $P700^T$ at room temperature [36].

The 206 μs time constant observed at 703 nm (Figure 5.2c), and the 60 μs time constant observed at 800 nm (Figure 6.5b) could also be due to the decay of $P700^{T}$. Another possibility, however, is that the 60–206 μs phase represents a direct recombination of $P700^{+}A_1^{-}$ to the singlet ground state. The recombination reaction populating the ground state rather than triplet state is the dominant process in WT PSI at low temperature when iron-sulfur clusters are pre-reduced [36]. The direct recombination of $P700^{+}A_1^{-}$ to the ground state is the dominant reaction at room temperature in WT PSI devoid of F_X, F_A, and F_B, and occurs with time constants of ~14 and 159 μs [13].

7 FORWARD ELECTRON TRANSFER FROM A_1 TO F_X IN WT AND *MENB* MUTANT PSI

Forward electron transfer from A_1^- to F_X in WT PSI is most easily probed at ~487 nm. What is probed at 487 nm is the absorption band of a carotenoid that is close to A_1. This carotenoid absorption band undergoes an electrochromic shift as the electron transfer between A_1^- and F_x procedes [10].

To study the A_1^- to F_X forward electron transfer process in WT and *menB* PSI transient absorption measurements probing at 487 nm were undertaken. The LP920 spectrometer set up is the same as described in previous chapters. Samples were suspended in 25 mM Tris buffer at pH 8.3. 0.04 % β-DM, 20 mM sodium ascorbate, 10 µM DCPIP, and 10 µM PMS were added. As pointed out above, PMS does not alter the photochemistry in the PSI particles, and is not strictly necessary. A 490 nm interference filter was placed in front of the sample, while a 480 nm interference filter was placed after the sample, in front of the monochromator entrance slit. The monochromator was set to transmit 487 nm. Spectral resolution is better than 2 nm. Measurements for both WT and *menB* PSI were made on 0.4, 2, 20, and 200 µs timescales. Measurements on *menB* PSI were also made on a 400 µs time scale. While both the probe and fluorescent background corrections were applied in measurements probing at 703 or 800 nm, only the probe background correction was necessary in measurements probing at 487 nm. This is because there is no fluorescence at 487 nm. All data is the average of multiple sets of 640 measurements.

Flash induced absorption changes for WT PSI particles at 487 nm, on four different time scales are shown in Figure 7.1. The data is fitted to either a single or double exponential

function. Calculated time constants are also shown in the figure 7.1. Electrical noise caused by the pump or probe shutter is present in the data on the 20 and 200 µs timescales. This noise does not affect any conclusions drawn from the data, however.

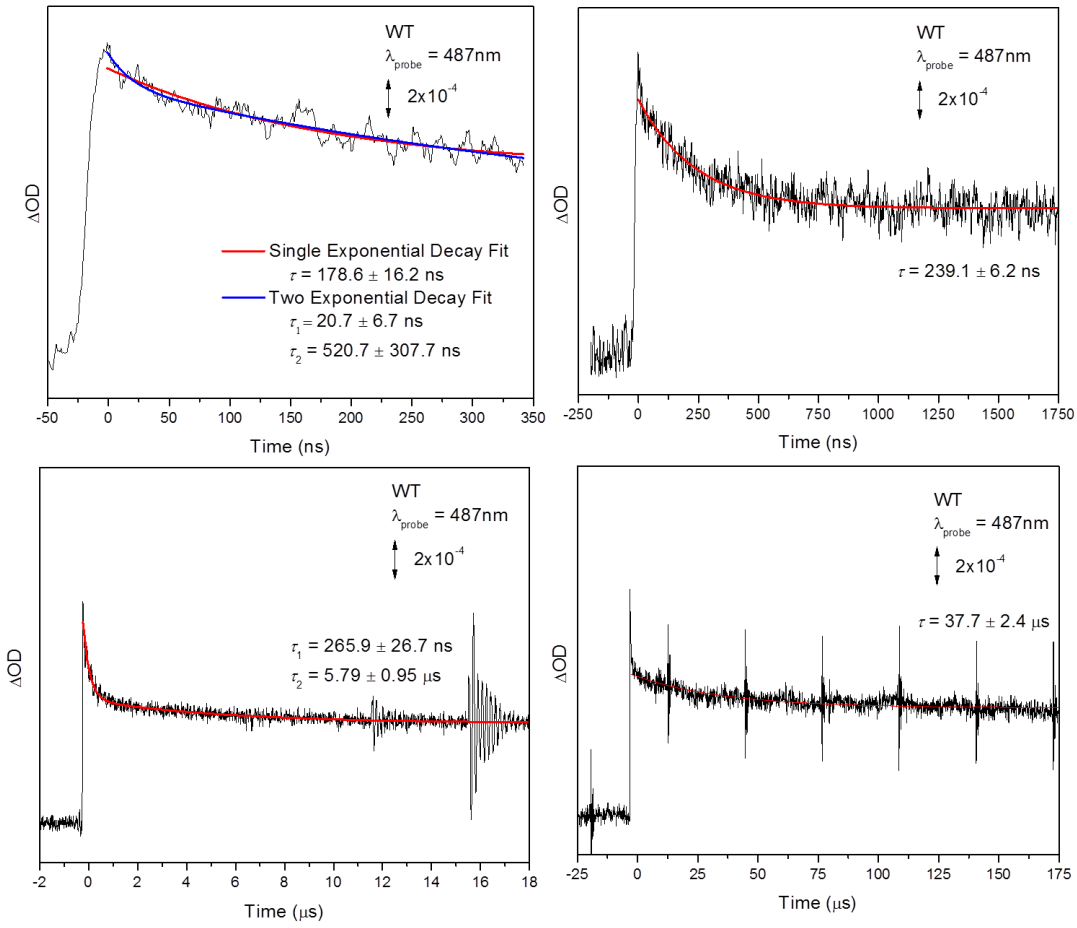

Figure 7.1 Flash induced absorption changes observed at 487 nm for WT PSI on a **a)** 400 ns, **b)** 2 µs, **c)** 20 µs, and **d)** 200µs timescale. Single and double exponential decay fits are also shown (*red* or *blue*).

According to previous studies, forward electron transfer from A_1^- to Fx is characterized by two time constants of ~20 ns and ~200 ns in WT PSI [37]. The data in Figure 7.1a-c indicates a decay phase with a lifetime between ~178-266 ns. The data in Figure 7.1a with a two exponential fit gives lifetimes of 20.7 ± 6.7 ns and 520.7 ± 307.7 ns. The fast phase is well

resolved. Clearly, however, the slow phase is not well-resolved since the time window of the measurement is too short. Based on the data in Figure 7.1b and c a time constant of approximately ~255 ns is obtained.

Flash induced absorption changes for *menB* PSI particles at 487 nm, on five different time scales are shown in Figure 7.2. The data is fitted to either a single or double exponential function. Calculated time constants are also shown in figure 7.2. Previously, for *menB* PSI, time constants of ~15 µs and ~250 µs were reported [22]. Figure 7.1 indicates that the kinetics in *menB* PSI are highly non-exponential. However, from figure 7.1c-e, a prominent decay phase with lifetime of 9-10 µs is observed. From figure 7.1e, a small amplitude decay phase with lifetime of 104 µs is also observed. So our work appears to be in line with these previous studies. We also observe decay phases with lifetimes in the ~100 – 700 ns range. Such decay phases were not observed previously, however.

In summary, from the measurements on WT and *menB* PSI at 487 nm on multiple time scales, two prominent decay phases are found for both WT and *menB* PSI. Presumably these phases represent forward electron transfer from A_1. For WT PSI, the time constants are 20.7 ± 6.7 ns and ~252.5 ns. For menB PSI, the time constant are ~9.6 µs, and ~103 µs. In addition, a sub-microsecond phase with a time constant of ~672 ns was also observed. The processes responsible for this latter decay phase is uncertain and is the subject of ongoing research.

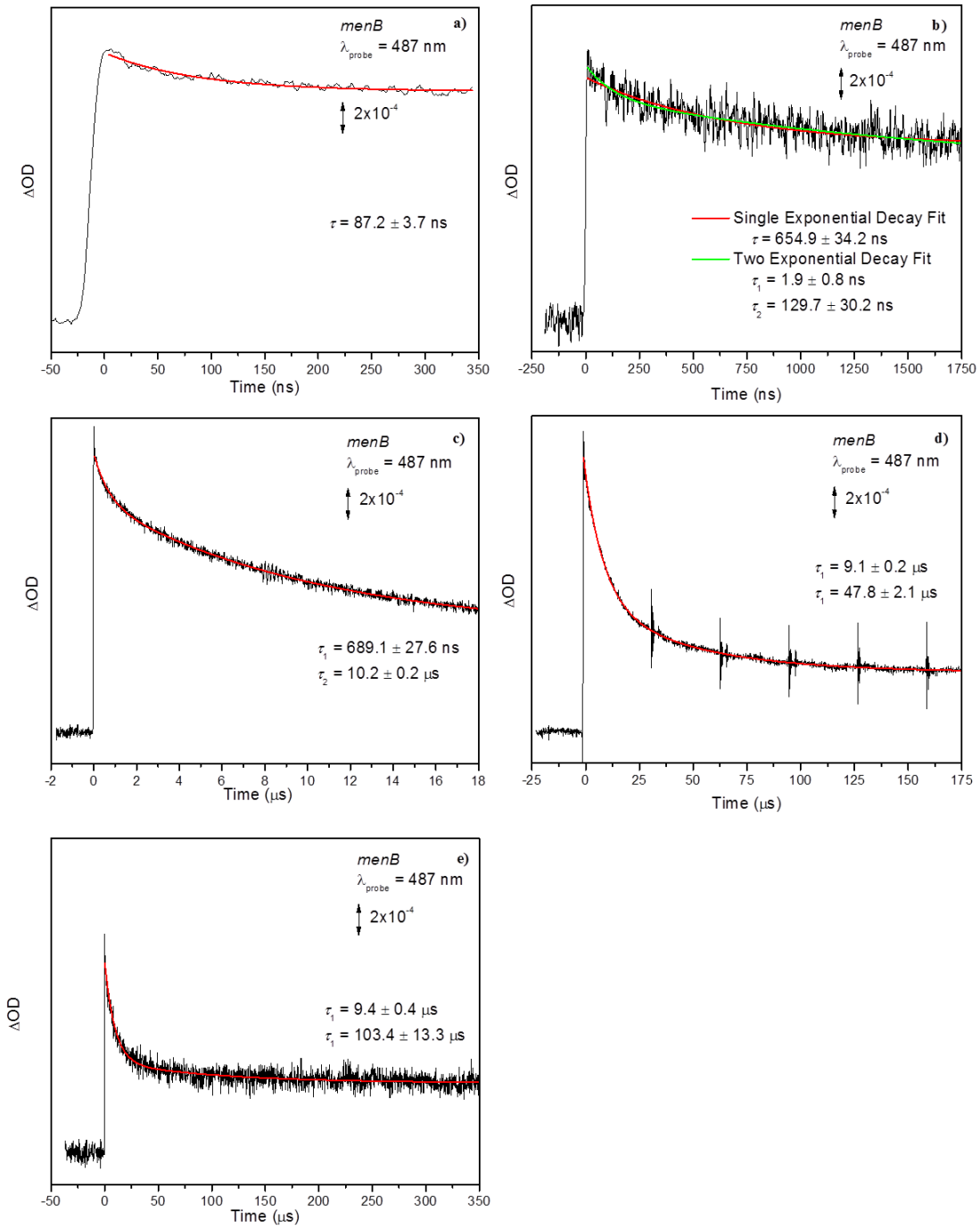

Figure 7.2 Flash induced absorption changes observed at 487 nm for menB PSI on a **a)** 400 ns, **b)** 2 μs, **c)** 20 μs, **d)** 200 μs and **e)** 400 μs timescale. Single and double exponential decay fits are also shown (*red* or *green*).

8 REPLACING PLASTOQUINONE WITH PHYLLOQUIONE IN *MENB* PSI.

The *menB* mutant is designed to disrupt certain genes involved in the biosynthetic pathway of phylloquinone [38, 39]. The idea was to create a system with an empty A_1 binding site, which would then allow the incorporation of foreign quinones, or the reincorporation of phylloquinone (PhQ). However, it was later found that the binding site was not empty, and that a foreign quinone had been recruited into the A_1 binding site. This quinone was identified as plastoquinones-9 (PQ). In previous chapters, we studied *menB* PSI with PQ in the A_1 binding site. Not unexpectedly, it was found that the kinetics of electron transfer in *menB* PSI differ markedly to that of WT PSI. PQ is loosely bound in the A_1 binding site, relative to PhQ, and it can be easily displaced by other quinones, either *in vivo* or *in vitro* [23].

In this chapter, we incubate *menB* PSI particles in the presence of PhQ, and we use pump-probe spectroscopy to study these pre-incubated samples, comparing the data to that obtained for both regular *menB* (with PQ) and with WT PSI.

The LP920 spectrometer was set up as described in previous chapters. Data were collected at 703, 800, and 487 nm. For *menB* PSI the reaction medium is the same as described previously (25 mM Tris, pH 8. 0.04 β-DM, 20 mM ascorbate, 10 µM DCPIP, and 10 µM PMS), except that PhQ was also added to the final concentration of 0.5 mM.

PhQ was added to *menB* PSI in proportion to the concentration of reaction centers. The concentration of reaction centers is determined by measuring the concentration of chlorophyll-*a* in the *menB* PSI reaction medium.

The procedure for measuring chlorophyll-a concentration is to take 10 µL of undiluted *menB* sample and mix it in 990 µL methanol. The UV-vis absorption spectrum of the mixture is taken, from which the concentration of chlorophyll-*a* in mg/mL is calculated using the equation:

$$c = \frac{A_{663} - A_{750}}{82} * f$$

A_{663} and A_{750} correspond to the optical densities at 663 nm and 750 nm respectively, and *f* is the dilution factor, which is 100 in this case. The concentration of reaction centers is calculated by deviding the chlorophyll-a concentration by 100, since there are ~100 chlorophyll-a molecules in the PSI particles. There are two quinone binding sites in the PSI reaction center. The targeted concentration of PhQ was 200 molecules for every A_1 binding site. PhQ dissolved in ethanol and added to the sample at less than 2 % v:v. *MenB* samples are incubated overnight in the dark in the presence of PhQ. Hereafter these samples are referred as *menB*+PhQ. Pump-probe measurements at 703, 800 and 487 nm were undertaken on a 400 ns time scale.

Figure 8.1 shows flash induced absorption changes at (a) 703 nm, (b) 800 nm, and (c) 487 nm, on a 400 ns timescale, for *menB*+PhQ PSI samples. Figure 8.1a-c show no significant absorption decay on this time scale. In particular in figure 8.1b, at 800 nm, no ~50 ns decay phase is observed. The lack of a 50 ns phase is characteristic of WT PSI (see Figure 6.2). This observation therefore demonstrates that PhQ has been reincorporated into *menB* PSI, and is functional in electron transfer, as it is in WT PSI.

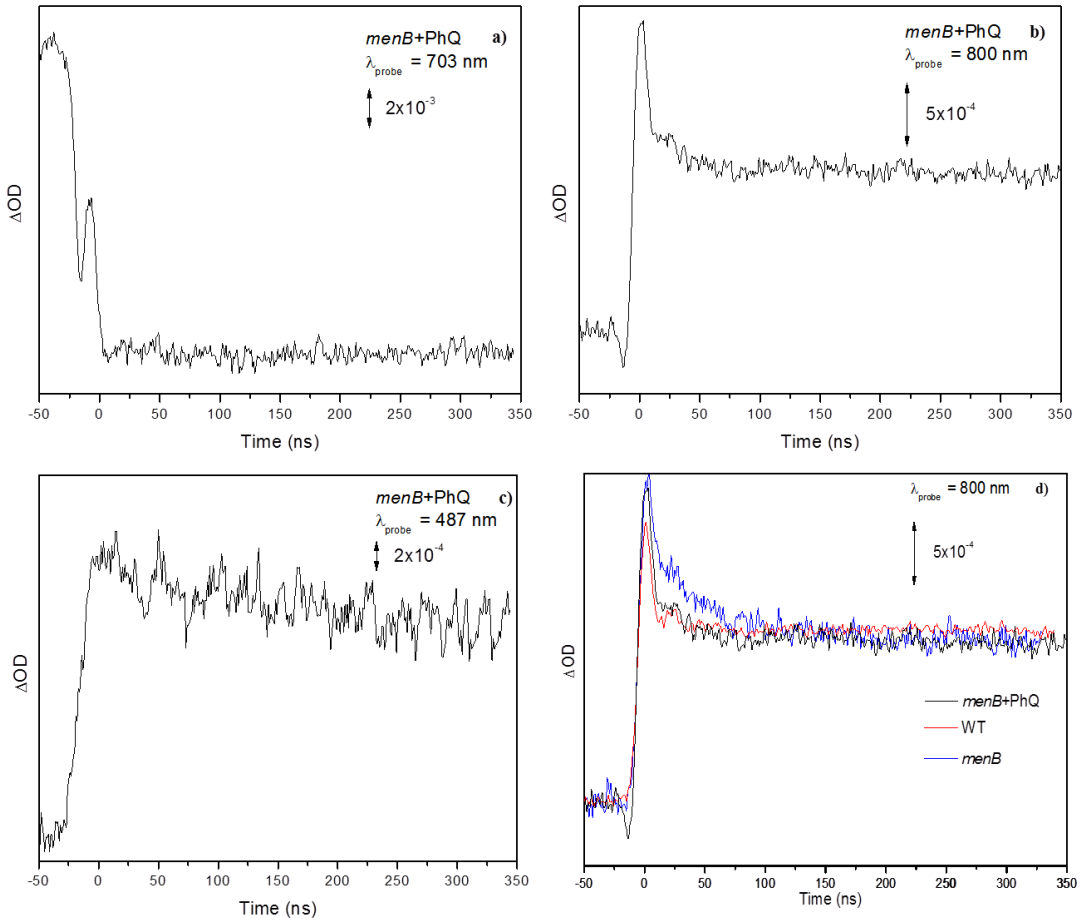

Figure 8.1 Flash induced absorption changes at **a)** 703 nm, **b)** 800 nm, and **c)** 487 nm on a 400 ns time scale for *menB*+PhQ PSI. **d)** Flash induced absorption changes at 800 nm for WT (*red*), menB (*blue*) and *menB*+PhQ (*black*) PSI samples.

At 703 nm (Figure 8.1a), unlike the *menB* trace which had a signal size smaller than the WT signal, the signal size is now even greater than the WT trace. Loss of the characteristic decay in *menB* at 800 nm and restoration of signal amplitude at 703 nm indicate that PhQ is incorporated in the A_1 binding site and that the samples regain the properties of WT samples. At 487 nm, due to a high noise level, whether the trace retains *menB* properties or gains WT properties could not be determined. Further experiments are underway to obtain data with improved signal to noise ratio. Figure 8.1.d shows a comparison of flash induced absorption

changes on a 400 ns timescale at 800 nm for *menB*, WT, and *menB*+PhQ PSI. The signal amplitudes of three traces were mutually normalized. Clearly *menB*+PhQ PSI closely resembles WT PSI, but is very different from *menB* PSI.

9 STUDY OF GREEN ALGAL PSI PARTICLES FROM *CHLAMMYDOMONAS REINHARDTII*.

Flash induced absorption changes at 487 nm were measured for PSI particles from *Chlamydomonas (C.) reinhardtii*. The previous chapters explained the settings of the spectrometer LP920. PSI from *C.reinhardtii* was suspended in 25 mM Tris buffer with 0.04 % β-DM at pH 8.3. The reaction medium contained: 20 mM sodium ascorbate, 10 μM DCPIP, and 10 μM PMS. The measurements were made at 487 nm in 400 ns, 1000 ns, and 2000 ns time scales.

Figure 9.1 shows flash induced absorbance changes at 487 nm measured using PSI particles from *C.reinhardtii.*PSI. Data were collected on three different time scales, which are all plotted in Figure 9.1. The data on all three timescales were fitted simultaneously to a double exponential function. The fits are also plotted in Figure 9.1.

The calculated lifetimes from global fitting of the data on three timescales are 31.9 ± 2.2 ns and 446.9 ± 18.7 ns. The decay rates are slightly slower than the rates determined for wild type *Synechocystis* sp. PCC 6803 under the same conditions. Guergova-Kuras et al. performed pump-probe spectroscopy on *C. reinhardtii* whole cells at 380 and 480 – 457 nm. The time constants obtained at 380 nm, where the absorption of the phyllosemiquinone is monitored, are ~19 ns and ~206 ns. At 480 – 457 nm, the spectral range of the electrochromic shift induced by A_1^-, the time constants ~19 ns and ~230 ns were reported [18]. Evans et al. monitored decay of the $P700^+A_1^-$ spin polarized signal by pulsed EPR spectroscopy at 260 K in membrane fragments of *C. reinhardtii* and reported a time constant ~512 ns [40].

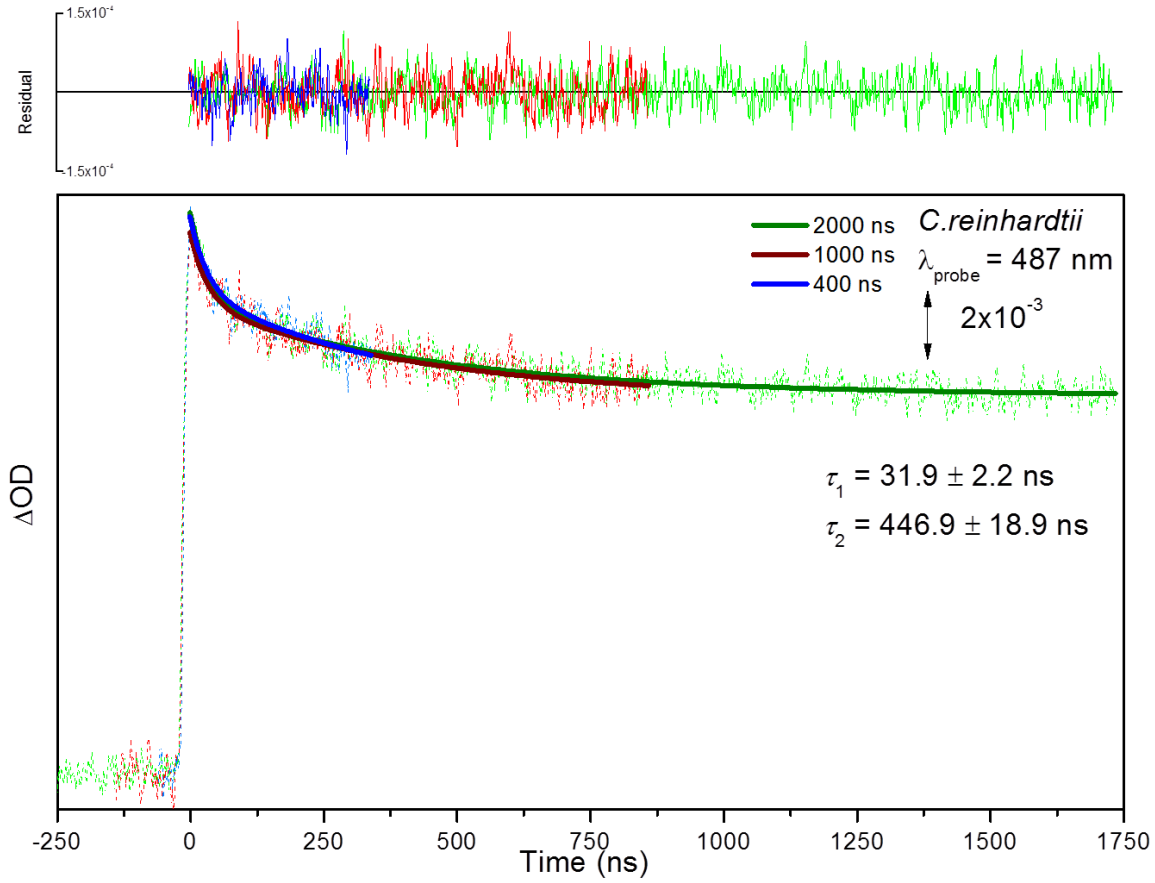

Figure 9.1 The traces of ΔOD of *C.reinhardtii* PSI observed at 487 nm in time scales 400 ns, 1000 ns, and 2000 ns with a global two exponential decay fitting on three traces. Solid lines indicate the fits, and dotted lines are the raw traces. Three residuals are also plotted together. τ_1 and τ_2 are the two mean-lifetime constants obtained from the global fitting.

10 STUDY OF CHLOROPHYLL-*D* CONTAINING PSI PARTICLES FROM *ACARYOCHLORIS MARINA*

Transient absorption spectroscopy is used to study electron transfer processes in chlorophyll-*d* containing PSI particles from *Acaryochloris (A.) marina*. Measurements were made at five different wavelengths between 465-512 nm. Lifetimes and nanosecond kinetic phases have been reported previously for whole cells PSI of A. marina [25]. Results have not been reported on isolated PSI particles, however. Analysis on the pump-probe spectroscopy measurements in this chapter resolves the lifetimes of the two phases and the ratio of the amplitudes at each wavelength.

The pump-probe spectroscopy was performed using the LP920 spectrometer with the set up described in previous chapters. Data were collected at 465, 487, 492, 505, and 512 nm. The wavelengths were selected using combinations of 480 nm interference filter, 490 nm interference filter, two 510 interference filters, and a monochromator. For 465 nm, interference filters (480 nm and 490 nm) were placed at an angle relative to the probe beam path. The sample, *A. marina*, was suspended in 25 mM Tris buffer with 0.04 % β-DM at pH 8.3. The reaction medium contained 20 mM sodium ascorbate, 10 µM DCPIP, and 10 µM PMS.

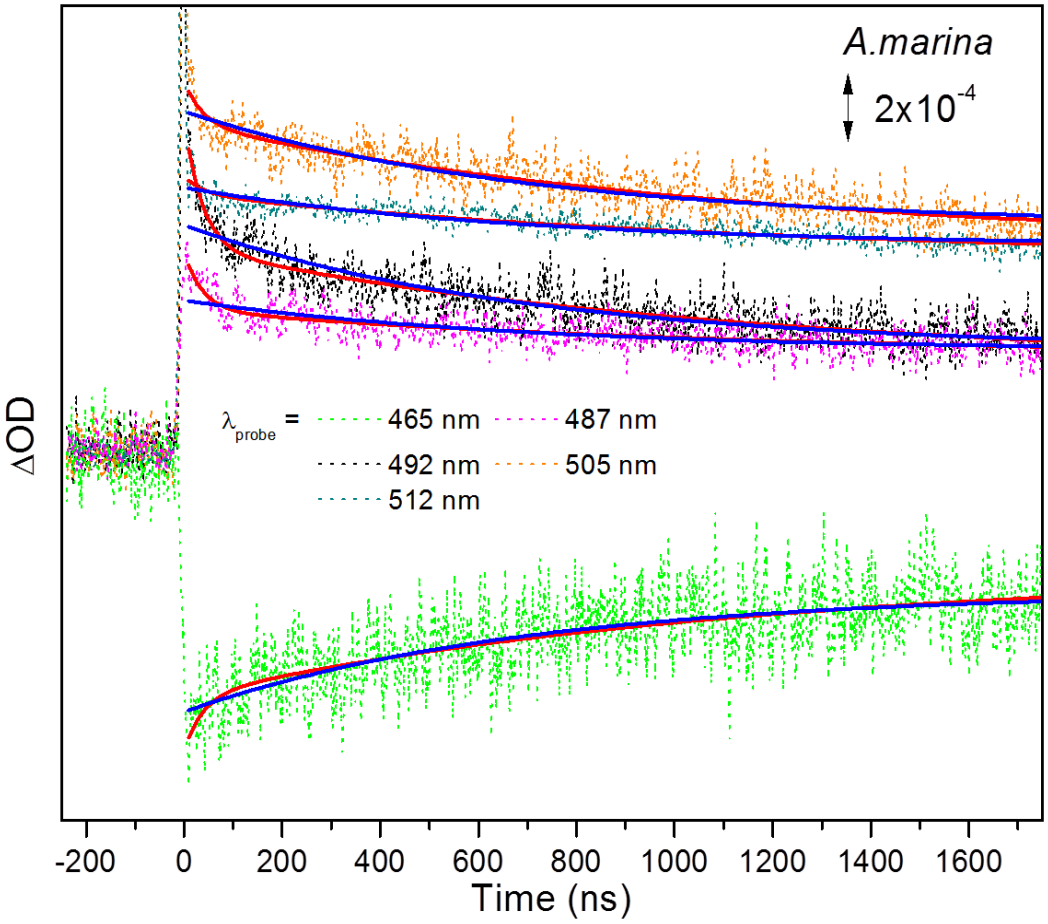

Figure 10.1 Global two exponential decay fitting on kinetics of *A. marina* observed at five different wavelengths (465, 487, 492, 505, and 512 nm) in 2000 ns time scale. Single exponential function (*blue*) and two exponential function (*red*) were fitted.

Table 10.1 Summary of calculated lifetimes obtained by fitting the kinetic data at 703 nm for *menB* PSI particles. The kinetics are associated with $P700^+$ charge recombination.

Fitted function		**Single exponential function**	**Two exponential function**	
Time constant(s)		$\tau = 697.6 \pm 20.6$ ns	$\tau_1 = 37.5 \pm 3.3$ ns	$\tau_2 = 1111.9 \pm 66.9$ ns
Amplitude	**465 nm**	-3.24×10^{-4}	-1.44×10^{-4}	-3.38×10^{-4}
	487 nm	1.35×10^{-4}	1.56×10^{-4}	1.24×10^{-4}
	492 nm	3.34×10^{-4}	3.44×10^{-4}	3.14×10^{-4}
	505 nm	3.07×10^{-4}	1.12×10^{-4}	3.30×10^{-4}
	512 nm	1.56×10^{-4}	4.62×10^{-5}	1.71×10^{-4}

Figure 10.1 shows flash induced absorption changes at 465, 487, 492, 505, and 512 nm, on a 2 μs timescale, obtained using PSI particles from *A. marina*. The data at the five wavelengths were fitted simultaneously to a two exponential function. The data and corresponding fits are shown in Figure 10.1. The fits yield lifetimes of 697.6 ± 20.6 ns with a single exponential function and 37.5 ± 3.3 ns and 1111.9 ± 66.9 ns with a two exponential function. The lifetimes reported by Santabarbara and co-workers were 88 ns and 345 ns [25]. The slow phase time constant calculated in this experiment follows the argument in Santabarbara's report that the forward electron transfer from A_1 occurs at slower rate compared to chlorophyll-*a* containing PSI. The fast phase from this experiment, however, decays at a rate similar to the chlorophyll-*a* containing PSI. The forward electron transfer rate of A_1 of chlorophyll-*d* containing PSI measured by the pump-probe spectroscopy on whole cells of PSI from *A.marina* have been reported by Santabarbara as mentioned already, yet the measurements on particle PSI from *A.marina* have not been reported. The differences in lifetimes of the two phases may be due to the conditions of PSI (particle or whole cells).

11 METHODS OF SELECTING PROBE LIGHT WAVELENGTH

As described in the chapter on my experiment's setup, the wavelength of the probe light is selected using interference filters, colored glasses, and a monochromator. Colored glasses, mostly long-pass filters, have a high transmission rate but a wide range of transmitted wavelengths. Although colored glasses can effectively block laser scattering while passing the wavelength of the interest, selecting a small range of wavelength by using colored glasses alone is not very effective. An interference filter is more suitable for selecting a small range of wavelengths. The full width at half maximum for many of the filters is less than 10 nm. However, the disadvantage of an interference filters also comes from its limited wavelength coverage range. Because each filter only covers a small range, covering a wide range of spectrum by only using interference filters is not cost effective. A monochromator on the other hand is able to select a specific wavelength from a wide range of wavelength. The disadvantage: on top of its cost, a lower transmission rate compared to interference filters and colored glasses because the beam is reflected off a mirror and diffraction gratings inside the monochromator. Therefore, a combination of interference filters, colored glasses, and monochromators need to be taken in consideration when selecting a wavelength for pump-probe spectroscopy.

In this chapter, a modification was made to LP920 system to use two monochromators instead of one, and its effectiveness was tested. The amount of light passed through, in terms of voltage measured by the photomultiplier detector, is compared.

In addition to the monochromator placed between the sample compartment and the PMT detector, an additional monochromator was placed between the probe lamp housing. The monochromator before the detector is the TMc300 by Bentham Instruments as described in Chapter 3. The voltage was measured at two wavelengths, 703 nm and at 487 nm. The bias

voltage on the PMT detector was set at 9.0, and the sample compartment contained no sample. The two interference filters used at 703 nm both have maximum peaks at 700 nm. The two interference filters used at 487 nm have one peak at 490 nm and the other with a peak at 480 nm. The voltage was measured when the probe light was tested in continuous wave mode and pulsed mode. Table 11.1 shows the result of the recorded voltage at each situation.

Table 11.1 Recorded voltage at 703 nm and at 487 nm under different set up

	703 nm	**487 nm**
2 monochromators, CW		
No filter	1.9×10^{-2}	7.5×10^{-2}
Orange colored glass	1.7×10^{-2}	5.2×10^{-2}
2 Monochromators, Pulsed		
No filter	5.1×10^{-2}	1.45
Orange colored glass	4.9×10^{-2}	1.45
1 Monochromator, CW		
2 Interference filters	1.8×10^{-1}	7.0×10^{-1}
1 Monochromator, CW		
2 Interference filters	$\gg 1$	$\gg 1$

As Table 11.1 shows, the voltage measured with one monochromator and two interference filters are orders of magnitude greater than the recorded voltage with two monochromators. Using a set up with combinations of interference filters, colored glasses, and a monochromator to select a wavelength is more effective as a lesser amount of light is lost than using two monochromators.

12 CONCLUSIONS

The laser flash photolysis technique, or the pump-probe spectroscopy, was applied to study the various kinetics of electron transfer in photosystem I. PSI particles from wild type *Synechocystis* sp. PCC 6803 and its mutant *menB* are studied in details at three wavelengths (703 nm, 800 nm, and 487 nm) in time scales ranging from 400 ns to 10 ms. The $P700^+$ charge recombination kinetics was observed at 700 nm and at 800 nm, where clear differences were seen between the traces of WT PSI and *menB* PSI. The signal's amplitude is smaller in *menB* traces at 703 nm, and a fast decay component with a time constant 30 – 50 ns. The kinetics trace of *menB* PSI at 703 nm was constructed from a nanosecond range to millisecond range in agreement with the previously reported kinetics trace of *menB* at 832 nm: the recombination kinetics with a decay rate ~2 ms and a minor decay phase of ~4 μs were obtained. The kinetics of the forward electron transfer from A_1 to F_X in wild type and *menB* PSI from *Synechocystis* sp. PCC 6803, PSI from *Chlamydomonas reinhardtii*, and *Acaryochloris marina* were probed with an intent to obtain the lifetimes of the fast and slow phase of the biphasic kinetics. From wild type *Synechocystis* sp. PCC 6803, two time constants were obtained 20.7 ± 6.7 ns and 252.5 ns, in agreement with the reported values of ~20 ns and ~200 ns [6]. The fast phase and slow phase of *menB* was calculated to have time constants ~9.6 μs and 103.4 ± 6.7 μs , slightly faster than the reported value of ~15 μs and 250 μs [22]. In addition to the biphasic kinetics components, a decay with a time constant ~672 ns was also observed. The exact mechanism of this decay has not been determined. Both fast and slow phases of the biphasic kinetics were determined from wild type particle PSI from *C.reinhardtii*: the fast phase has a time constant 31.9 ± 2.2 ns, and the slow phase has a time constant 446.9 ± 18.9 ns. Lastly, the kinetics of the particle PSI from *Acaryochloris marina* was observed at multiple wavelengths to investigate its biphasic kinetics.

Although the kinetics was studied in whole cells PSI previously, particle PSI has not been investigated before. The time constants are obtained through global fits as 697.6 ± 20.6 ns with a single exponential function and 37.5 ± 3.3 ns and 1111.9 ± 66.9 ns with a two exponential function. The two time constants deviate from the constants reported on whole cells PSI, which were 88 ns and 345 ns [25].

The future research area includes unknown decay phases in *menB* PSI at 800 nm and at 487 nm. The phases are distinctly observed in *menB* but not in WT, and the mechanisms are not understood. As a continuation to the experiment of the restoration of phylloquinone in *menB* PSI, other quinones may be added to fill the A_1 binding site and study its effect in the kinetics. Some of the quinones that may be added are naphthoquinone and anthraquinone. The research on *Acaryochloris marina* includes measurements at more wavelengths and in more time scales to investigate the biphasic kinetics in more details. The pump-probe spectroscopy may also be applied to study the $P740^+$ charge recombination kinetics to further the understanding of the electron transfer in chlorophyll-*d* containing PSI.

REFERENCES

1. Nield, J. *Schematic models for the major protein complexes involved in photosynthesis*. 2011; Available from: http://www.photosynthesis.sbcs.qmul.ac.uk/nield/psIIimages/oxygenicphotosynthmodel.html.
2. Fromme, P., Jordan, P., and Krauss, N., *Structure of photosystem I.* Biochimica et Biophysica Acta (BBA) - Bioenergetics, 2001. **1507**(1-3): p. 5-31.
3. Nield, J., *Light-harvesting I - Photosystem I complex (LHCI-PSI).* 2011.
4. Shinkarev, V.P., Zybailov, B., Vassiliev, I.R., and Golbeck, J.H., *Modeling of the P700+ Charge Recombination Kinetics with Phylloquinone and Plastoquinone-9 in the A1 Site of Photosystem I.* Biophysical Journal, 2002. **83**(6): p. 2885-2897.
5. van der Est, A. and Golbeck, J.H., *Electron Transfer Involving Phylloquinone in Photosystem I: Photosystem I*. 2006, Springer Netherlands. p. 387-411.
6. Brettel, K. and Leibl, W., *Electron transfer in photosystem I.* Biochimica et Biophysica Acta (BBA) - Bioenergetics, 2001. **1507**(1-3): p. 100-114.
7. Hastings, G., Kleinherenbrink, F.A.M., Lin, S., McHugh, T.J., and Blankenship, R.E., *Observation of the Reduction and Reoxidation of the Primary Electron Acceptor in Photosystem I.* Biochemistry, 1994. **33**(11): p. 3193-3200.
8. Setif, P., Bottin, H., and Mathis, P., *Absorption studies of primary reactions in Photosystem I. Yield and rate of formation of the P-700 triplet state.* Biochimica et Biophysica Acta (BBA) - Bioenergetics, 1985. **808**(1): p. 112-122.
9. Setif, P. and Brettel, K., *Forward electron transfer from phylloquinone A1 to iron-sulfur centers in spinach photosystem I.* Biochemistry, 1993. **32**(31): p. 7846-7854.
10. Bautista, J.A., Rappaport, F., Guergova-Kuras, M., Cohen, R.O., Golbeck, J.H., Wang, J.Y., Beal, D., and Diner, B.A., *Biochemical and Biophysical Characterization of Photosystem I from Phytoene Desaturase and Zeta-Carotene Desaturase Deletion Mutants of Synechocystis Sp. PCC 6803: evidence for PsaA- and PsaB-side electron transport in cyanobacteria.* Journal of Biological Chemistry, 2005. **280**(20): p. 20030-20041.
11. Brettel, K., *Electron transfer from A1 to an iron-sulfur center with t12 = 200 ns at room temperature in photosystem I Characterization by flash absorption spectroscopy.* FEBS Letters, 1988. **239**(1): p. 93-98.
12. Agalarov, R. and Brettel, K., *Temperature dependence of biphasic forward electron transfer from the phylloquinone(s) A1 in photosystem I: only the slower phase is activated.* Biochimica et Biophysica Acta (BBA) - Bioenergetics, 2003. **1604**(1): p. 7-12.
13. Brettel, K. and Golbeck, J.H., *Spectral and kinetic characterization of electron acceptor A1 in a Photosystem I core devoid of iron-sulfur centers FX, FB and FA.* Photosynthesis Research, 1995. **45**(3): p. 183-193.
14. Brettel, K., Setif, P., and Mathis, P., *Flash-induced absorption changes in photosystem I at low temperature: evidence that the electron acceptor A1 is vitamin K1.* FEBS Letters, 1986. **203**(2): p. 220-224.
15. Setif, P. and Brettel, K., *Photosystem I photochemistry under highly reducing conditions: Study of the P700 triplet state formation from the secondary radical pair (P700+A1-).* Biochimica et Biophysica Acta (BBA) - Bioenergetics, 1990. **1020**(3): p. 232-238.

16. Redding, K., van der Est, A., and Golbeck, J.H., *The Directionality of Electron Transport in Photosystem I: Photosystem I.* 2006, Springer Netherlands. p. 413-437.
17. Joliot, P. and Joliot, A., *In Vivo Analysis of the Electron Transfer within Photosystem I: Are the Two Phylloquinones Involved?* Biochemistry, 1999. **38**(34): p. 11130-11136.
18. Guergova-Kuras, M., Boudreaux, B., Joliot, A., Joliot, P., and Redding, K., *Evidence for two active branches for electron transfer in photosystem I.* Proceedings of the National Academy of Sciences, 2001. **98**(8): p. 4437-4442.
19. Cohen, R.O., Shen, G., Golbeck, J.H., Xu, W., Chitnis, P.R., Valieva, A.I., van der Est, A., Pushkar, Y., and Stehlik, D., *Evidence for Asymmetric Electron Transfer in Cyanobacterial Photosystem I: Analysis of a Methionine-to-Leucine Mutation of the Ligand to the Primary Electron Acceptor A0.* Biochemistry, 2004. **43**(16): p. 4741-4754.
20. Fairclough, W.V., Forsyth, A., Evans, M.C.W., Rigby, S.E.J., Purton, S., and Heathcote, P., *Bidirectional electron transfer in photosystem I: electron transfer on the PsaA side is not essential for phototrophic growth in Chlamydomonas.* Biochimica et Biophysica Acta (BBA) - Bioenergetics, 2003. **1606**(1-3): p. 43-55.
21. Ramesh, V.M., Gibasiewicz, K., Lin, S., Bingham, S.E., and Webber, A.N., *Bidirectional Electron Transfer in Photosystem I: Accumulation of A0- in A-Side or B-Side Mutants of the Axial Ligand to Chlorophyll A0.* Biochemistry, 2004. **43**(5): p. 1369-1375.
22. Semenov, A.Y., Vassiliev, I.R., van der Est, A., Mamedov, M.D., Zybailov, B., Shen, G., Stehlik, D., Diner, B.A., Chitnis, P.R., and Golbeck, J.H., *Recruitment of a Foreign Quinone into the A1 Site of Photosystem I.* Journal of Biological Chemistry, 2000. **275**(31): p. 23429-23438.
23. Johnson, T.W., Shen, G., Zybailov, B., Kolling, D., Reategui, R., Beauparlant, S., Vassiliev, I.R., Bryant, D.A., Jones, A.D., Golbeck, J.H., and Chitnis, P.R., *Recruitment of a Foreign Quinone into the A1 Site of Photosystem I.* Journal of Biological Chemistry, 2000. **275**(12): p. 8523-8530.
24. Schenderlein, M., Cetin, M., Barber, J., Telfer, A., and Schlodder, E., *Spectroscopic studies of the chlorophyll d containing photosystem I from the cyanobacterium, Acaryochloris marina.* Biochimica et Biophysica Acta (BBA) - Bioenergetics, 2008. **1777**(11): p. 1400-1408.
25. Santabarbara, S., Bailleul, B., Redding, K., Barber, J., Rappaport, F., and Telfer, A., *Kinetics of phyllosemiquinone oxidation in the Photosystem I reaction centre of Acaryochloris marina.* Biochimica et Biophysica Acta (BBA) - Bioenergetics. **1817**(2): p. 328-335.
26. Porter, G., *Flash Photolysis and Some of Its Applications.* Nobel Lecture, 1967.
27. Wientjes, E. and Croce, R., *PMS: Photosystem I electron donor or fluorescence quencher.* Photosynthesis Research. **111**(1): p. 185-191.
28. Dashdorj, N., Xu, W., Martinsson, P., Chitnis, P.R., and Savikhin, S., *Electrochromic Shift of Chlorophyll Absorption in Photosystem I from Synechocystis sp. PCC 6803: A Probe of Optical and Dielectric Properties around the Secondary Electron Acceptor.* Biophysical Journal, 2004. **86**(5): p. 3121-3130.
29. Edinburgh Instruments, L., *Operating Instructions LP920 Laser Flash Photolysis Spectrometer*. 2008.
30. Chauvet, A., Dashdorj, N., Golbeck, J.H., Johnson, T.W., and Savikhin, S., *Spectral Resolution of the Primary Electron Acceptor A0 in Photosystem I.* The Journal of Physical Chemistry B. **116**(10): p. 3380-3386.

31. Brettel, K., *Electron transfer and arrangement of the redox cofactors in photosystem I.* Biochim. Biophys. Acta, 1997. **1318**(3): p. 322-373.
32. Golbeck, J.H. and Bryant, D., *Photosystem I,* in *Current topics in bioenergetics*. 1991, Academic Press: New York. p. 83-175.
33. Setif, P., Hervo, G., and Mathis, P., *Flash-induced absorption changes in Photosystem I, Radical pair or triplet state formation?* Biochimica et Biophysica Acta (BBA) - Bioenergetics, 1981. **638**(2): p. 257-267.
34. Cassan, N., Lagoutte, B., and Setif, P., *Ferredoxin-NADP+ reductase : Kinetics of electron transfer, transient intermediates and catalytic activities studied by flash-absorption spectroscopy with isolated photosystem-I and ferredoxin.* Journal of Biological Chemistry, 2005.
35. Noguchi, T., Tomo, T., and Kato, C., *Triplet Formation on a Monomeric Chlorophyll in the Photosystem II Reaction Center As Studied by Time-Resolved Infrared Spectroscopy.* Biochemistry, 2001. **40**(7): p. 2176-2185.
36. Polm, M. and Brettel, K., *Secondary Pair Charge Recombination in Photosystem I under Strongly Reducing Conditions: Temperature Dependence and Suggested Mechanism.* Biophysical Journal, 1998. **74**(6): p. 3173-3181.
37. Agalarov, R. and Brettel, K., *Temperature dependence of biphasic forward electron transfer from the phylloquinone(s) A1 in photosystem I: only the slower phase is activated.* Biochim. Biophys. Acta, 2003. **1604**(1): p. 7-12.
38. Johnson, T.W., Shen, G., Zybailov, B., Kolling, D., Reategui, R., Beauparlant, S., Vassiliev, I.R., Bryant, D.A., Jones, A.D., Golbeck, J.H., and Chitnis, P.R., *Recruitment of a foreign quinone into the A_1 site of photosystem I. I. Genetic and physiological characterization of phylloquinone biosynthetic pathway mutants in Synechocystis sp. pcc 6803.* J. Biol. Chem., 2000. **275**(12): p. 8523-8530.
39. Johnson, T.W., Zybailov, B., Jones, A.D., Bittl, R., Zech, S., Stehlik, D., Golbeck, J.H., and Chitnis, P.R., *Recruitment of a foreign quinone into the A_1 site of photosystem I. In vivo replacement of plastoquinone-9 by media-supplemented naphthoquinones in phylloquinone biosynthetic pathway mutants of Synechocystis sp. PCC 6803.* J. Biol. Chem., 2001. **276**(43): p. 39512-39521.
40. Evans, M.C.W., Purton, S., Patel, V., Wright, D., Heathcote, P., and Rigby, S.E.J., *Modification of electron transfer from the quinone electron carrier, A1, of Photosystem 1 in a site directed mutant D576→L within the Fe-Sx binding site of PsaA and in second site suppressors of the mutation in Chlamydomonas reinhardtii.* Photosynthesis Research, 1999. **61**(1): p. 33-42.